QUANTITATIVE *E. COLI* DETECTION ON GELATIN-BASED MICROFLUIDIC UNDER AN ENZYMATIC REACTION FOR FLUORESCENT PRODUCT AND THE SIMULATION FOR THE *E. COLI* DETECTION LIMIT BY THE SURFACE PLASMON RESONANCE USING THE EFFECTIVE REFLECTIVE INDEX THEORY

BY

CHANIN LOCHOTINUNT

A THESIS SUBMITTED IN PARTIAL FULFILLMENT

OF THE REQUIREMENT FOR THE DEGREE OF

MASTER OF ENGINEERING IN BIOMEDICAL ENGINEERING

SCHOOL OF ENGINEERING

KING MONGKUT'S INSTITUTE OF TECHNOLOGY LADKRABANG

2022

KMITL-2023-EN-M-317-003

QUANTITATIVE *E. COLI* DETECTION ON GELATIN-BASED MICROFLUIDIC UNDER AN ENZYMATIC REACTION FOR FLUORESCENT PRODUCT AND THE SIMULATION FOR THE *E. COLI* DETECTION LIMIT BY THE SURFACE PLASMON RESONANCE USING THE EFFECTIVE REFLECTIVE INDEX THEORY

CHANIN LOCHOTINUNT

A THESIS SUBMITTED IN PARTIAL FULFILLMENT

OF THE REQUIREMENT FOR THE DEGREE OF

MASTER OF ENGINEERING IN BIOMEDICAL ENGINEERING

SCHOOL OF ENGINEERING

KING MONGKUT'S INSTITUTE OF TECHNOLOGY LADKRABANG

2022

KMITL-2023-EN-M-317-003

Thesis	Quantitative *E. coli* detection on gelatin-based microfluidic under an enzymatic reaction for fluorescent product and the simulation for the *E. coli* detection limit by the surface plasmon resonance using the effective reflective index theory
Student	Mr. Chanin Lochotinunt
Student ID.	64601031
Degree	Master of Engineering
Program	Biomedical Engineering
Year	2022
Thesis Advisor	Asst. Prof. Dr. Treesukon Treebupachatsakul
Thesis Co-Advisor	Assoc. Prof. Dr. Suejit Pechprasarn

ABSTRACT

Escherichia coli (*E. coli*) contamination in food product issues has existed for a long time. Therefore, foodborne pathogen standard in food products has developed a detection method. The *E. coli* detection method nowadays has various techniques; however, the most general detection method based on enzymatic reaction is detecting *E. coli* from biomarker, which is enzyme activity secreted from *E. coli*. In this thesis research, the blue fluorescence emitted by 4-methyl-umbelliferone (4MU) was used to quantify the number of *E. coli* colonies. The enzyme β-D-glucuronidase (GUD), which is secreted by various strains of *E. coli*, and its substrate 4-methylumbelliferyl- β-D-glucuronide (MUG), catalyzes a reaction to produce the 4MU. This thesis has used this enzymatic reaction and provided straightforward technology for label-free, in-situ, quantitative *E. coli* detection. This detecting platform setup includes a MUG-suspended gelatin-based microfluidic channel, smartphone camera, and ultraviolet light source. The proposed *E. coli* detection mechanism is the passive diffusion of secreted GUD enzyme and the MUG substrate suspended in the gelatin. In addition, this research has also presented a laser printer-based fabrication technique for creating the MUG-suspended gelatin microfluidic channels. This research demonstrated that the 4MU fluorescence emission, which was stimulated by the UV light on the gelatin film, can be recorded using a smartphone

camera. As the base-line signal, distilled water was also employed as a negative control, while 1700 U/ml of the GUD enzyme served as a positive control. Due to the delay of the diffusion mechanism and the enzymatic reaction, the detection framework required at least 2 hours to detect the fluorescence product from cultivated *E. coli* at a variable concentration under the gelatin channel with the sensor readout time below 7 seconds. *E. coli* colonies can be counted using the indicated *E. coli* detection method without sophisticated equipment, cell culture, inoculation, or liquid sample. Additionally, the proposed method has a trade-off between reaction time and detection limit.

Surface plasmon resonance has traditionally been the standard method for label-free biomedical and biochemical measures, including protein binding kinetics and protein-protein interactions. The theory of surface plasmon resonance has a strong basis and has proven to be extremely sensitive to detecting tiny molecules, proteins, and nucleotides. However, the *E. coli* surface plasmon resonance detection results have not yet demonstrated an outstanding detection limit. Around 10^3 CFU/ml is the average *E. coli* detection limit using the traditional surface plasmon platform. A secondary binding agent to *E. coli*, such as conjugated nanoparticles, can increase the detection limit of the SPR sensor. So, I have proposed a theoretical framework based on effective refractive index theory to explain the detection method and provide insight into the underlying challenges that reduce the detection limit of surface plasmon resonance. The effective refractive index model based on the Kretschmann configuration was applied to find the detection limit of surface plasmon resonance for detecting *E. coli*. I have used the experimental result to validate the model from Vaisocherová-Lísalová *et al.* [1] literature. The result was that the simulation using an effective refractive index model shows good agreement with the 2 cases of experimental results of the Vaisocherová-Lísalová *et al.* literature. We discovered from the investigation that the thickness of the binding site could decrease the sensitivity, and the detection limit was around $10^{2.807}$-$10^{3.424}$ CFU/ml.

ACKNOWLEDGEMENTS

First of all, I would like to express my deepest appreciation to my advisor, Asst. Prof. Dr. Treesukon Treebupachatsakul has provided me with continuous support, immense knowledge, and access to the laboratory and research facilities and guided me throughout this master's degree research project. Without their assistance in every step throughout the process, this research project would have never been accomplished.

I would like to express my sincere gratitude to Assoc. Prof. Dr. Suejit Pechprasarn gave advice, insightful comments, and encouragement. Without his advice, this research would not be possible to accomplish.

Further, I would also like to express my gratitude to my previous bachelor's research partner, Miss Thitirat Teechot, for studying the Microfluidic channel from gelatin with me in my bachelor's degree, which I have applied to this research project. I am also grateful to Dr. Nattha Pensupa for giving me a comment and advice on my journal paper. To conclude, I cannot forget to thank my family and friends for all the unconditional support during this very intense academic year.

I acknowledge research funding supported by a scholarship from King Mongkut's Institute of Technology Ladkrabang, contract number KREF016413, and the College of Biomedical Engineering, Rangsit University (RSU).

Chanin Lochotinunt

TABLE OF CONTENTS

Page

LIST OF TABLES

Table Page

LIST OF FIGURES

Figure **Page**

LIST OF SYMBOLS / ABBREVIATIONS

Symbols/Abbreviations	Terms
GUD	β-D-glucuronidase
MUG	4-methylumbelliferyl-β-D-glucuronide
4MU	4-methylumbelliferone
E. coli	*Escherichia coli*
UV	Ultraviolet
CFU	Colony-forming units
SPR	Surface Plasmon Resonance
LoD	Limit of detection

CHAPTER 1
INTRODUCTION

1.1 Background and Significance of the research

Foodborne pathogens consist of bacteria, parasites, or even viruses that can cause a foodborne illness by contaminating food and consumption. *Escherichia coli*, or *E. coli*, are typical foodborne pathogens. Generally, *E. coli* can be discovered in the digestive tract of warm-blood animals and humans. However, *E. coli* can cause a foodborne illness due to its high concentration. The symptoms that occur from consuming some *E. coli* strain contaminated in food can range from mild to severe such as diarrhea, stomach pain, nausea, vomiting, *etc.* [2]. *E. coli* infection in humans can also be brought on by consuming contaminated food and drinking water, such as undercooked or raw meat products, fresh products like vegetables, and unpasteurized or fresh milk contaminated with the pathogen [3, 4]. In 2011, an *E. coli* outbreak in Central Europe caused around 4,000 people to be infected, over 900 of Hemolytic Uremic Syndrome (HUS), which damages an infected person's kidney and blood clotting capabilities, and 54 deaths [5, 6]. Therefore, one of the biggest problems facing the agricultural industry involves the issue of food safety. *E. coli* contamination in food products can be an indicator of hygiene that public health focuses on and is concerned about. At the same time, bacterial contamination can also happen at any point in the food supply chain. Bacteriological verification and prevention are required to decrease the danger of bacterial contamination that can result in dangerous infections. Microbiological screening and avoidance are essential in order to decrease the severe chance of bacterial infection, which can cause life-threatening illness. According to ISO 9308-1:2014 (the International Organization for Standardization), drinking water, decontaminated pool water, or completed water from water treatment plants must contain coliform bacteria, including *E. coli*, with less than 100 total colonies on chromogenic coliform agar [7]. The World Health Organization also has defined safe drinking water as having 0 *E. coli* per 100 ml of water, 1-10 MPN/100 ml as riskless, 11-100 MPN/100 ml as a medium risk, and more than 100 MPN/100 ml as hazardous [8].

There are several *E. coli* detection methods that have been reported. In Table 1.1, I have reviewed and summarized the usual time of *E. coli* detection techniques. The detection time ranges from around 16-1 hour, 12 hours, a day, several days, or a week depending on the technique. The proposed technique takes 2 to 3 hours, which is better than most of the methods described in the literature, as will be demonstrated and discussed later. The fact that it can be performed in situ without the need for cell culture or inoculation gives it significant advantages over other analytical techniques, even though it does not demonstrate an excellent response time compared to those analytical techniques with a response time of less than an hour. The proposed method might be a preferable option in the future for packaging technology coupled with an *E. coli* detection mechanism when compared to the published analytical techniques.

Table 1.1 Show the detection limit with the detection time for several *E. coli* detection techniques

Method	Detection limit	Detection time	Reference
Plating/culturing	Low CFUs	1 day to 1 week	Deisingh AK *et al*. [9]
Biochemical tests	Low CFUs	1 day to several days	
ELISA	10-100 CFU/ml	12 hours to 2 days	
Fluorescent bacteriophage assay	10-100 CFU/ml	10 hours	
Time-resolved fluorescence immunoassay	10-100 CFU/ml	6 hours	
Capillary immunoassay	0.5-1 CFU/ml	7 hours	
PCR	10^2-10^5 CFU/ml	2–24 hours, depending on the enrichment	
Integrated systems (lab-on-a-chip)	10^2-10^4 CFU/ml	16-45 minutes	
RT - PCR	10^7 CFU/ml	6-12 hours	

Microarrays	55 CFU/ml	Less than 1 hour	
SPR biosensor	$5x10^7$ CFU/ml	1 hour	
Molecular beacon	$1\text{-}10^3$ CFU/ml	1–6 hours, depending on the enrichment	
Multiplex PCR	1-2 CFU/ml	24 hours	
Quantum dot	5-10 CFU/ml	1 hour and 20 minutes	Hongying Zhu *et al.* [10]
FTIR nano biosensors	$1x10^2$ CFU/ml	30 minutes	Stefania Mura *et al.* [11]
Nano platinum-graphene paper aptasensor	4 CFU/ml	12 minutes	Yu-Wen Zhao *et al.* [12]
Hand-held fluorescence detector	$10^2\text{-}10^8$ CFU/ml	30 minutes	Wildeboer *et al.* [13]
Sorbitol MacConkey agar (SMAC) medium	Low CFUs	24 hours	S B March *et al.* [14]
Membrane-Based Electrochemical Nanobiosensor	$10\text{-}10^6$ CFU/ml	90 minutes	Ming Soon Cheng *et al.* [15]

The catalytic reaction is widely used for investigating the *E. coli* from the enzyme of β-D-glucuronidase (GUD) activity produced by *E. coli* and binds explicitly with substrate 4-methylumbelliferyl-β-D-glucuronide (MUG) to form the blue fluorescence product 4-methyl-umbelliferone (4MU) [16]. Furthermore, the GUD enzyme is produced by 94–96% of the *E. coli* strains [17, 18]. The GUD enzyme could therefore be employed as a fluorescence biomarker to differentiate between different strains of *E. coli* [19]. The 4MU fluorescence intensity could be used to quantify the quantity of *E. coli*, similar to the rt-PCR method [13],

by examining the fluorescence in the conventional medium that added MUG substance under the ultraviolet light (UV) [20, 21].

This research aims to develop a fluorescence-based technique that can detect *E. coli* by measuring the activity of the GUD enzyme from the emitted blue fluorescence under the substrate MUG suspended in a gelatin-based microfluidic channel. In this research, the simple hardware MUG suspended gelatin-based microfluidic was fabricated for detecting *E. coli* from the blue fluorescence of the catalytic reaction product. The components that are required for this platform consist of (1) a MUG-suspended gelatin microfluidic channel, (2) a smartphone camera for recording fluorescence signal, (3) a UV light source for stimulated fluorescence product, and (4) a sample. As a result of the gelatin channels being indirect contact with the sample, the liquid sample can be drawn into the microchannels by passive capillary force due to the tiny channel size. Here, the *E. coli* produced GUD enzyme can pass through the permeability gelatin material and react with the MUG substrate in gelatin to form a blue fluorescence 4MU product. Quantitative detection of *E. coli* is possible due to the blue fluorescence intensity's relationship to *E. coli* concentration. The 4MU can be excited and emitted at a wavelength of 355 and 450 nm, respectively, under the UV light source [13]. Without the requirement for an extra optical filter, the 2 mm of gelatin fluidic channel and smartphone camera can filter UV background light and record the 4MU fluorescence light, which will be reported later.

Here, the presented *E. coli* detection platform has different features over previous 4MU-based techniques [22], such as (1) A simple, cheap, and environmentally friendly production method can fabricate the MUG-suspended gelatin-based microfluidic channel. (2) The reaction channel requires a smaller sample volume of about 0.3 ml, proceeded on lab-on-a-chip microfluidic technology. (3) Complex equipment is not necessary. Moreover, (4) The smartphone camera can quantify fluorescence emission and compare it to GUD activity in the colony-forming unit (CFU/ml), allowing for the quantitatively rapid detection of *E. coli*.

The Surface plasmon resonance (SPR) is a restricted electromagnetic wave phenomenon that occurs on the surface of noble metals like silver (Ag), copper (Cu), and gold (Au) [23]. Various *E. coli* detection techniques have been developed and reported. The SPR is also one of the recent and low-cost used in the foodborne pathogens detection

technique, including *E. coli* [24, 25]. The conventional SPR setup, also known as the Kretschmann configuration, is the widely used procedure for surface plasmon measurement. According to the Kretschmann configuration, polarized coherent light is used to illuminate the plasmonic sensor through a prism and then reflect off a metal surface. An optical camera or a photodiode can be used to measure the reflectance. Even though the theory underlying SPR is relatively well known, it has not been researched why the SPR is unfavourable for food pathogens. Therefore, using optical simulation and modelling, the following theoretical analysis was suggested to explain the impacts of each component in the SPR sensor on the detection limit and the sensitivity of the SPR for *E. coli* detection. This has never been documented in the literature, as far as my knowledge.

1.2 Objectives

1. Apply gelatin-based microfluidics for *E. coli* detection under enzymatic reaction.
2. To investigate the relation between the amount of *E. coli* and fluorescence product collected from a smartphone.
3. To express the rapid *E. coli* detection by using a smartphone camera.
4. To find the detection limit of surface plasmon resonance for *E. coli* detection.

1.3 Research hypothesis

1. Microfluidic made from gelatin can be used as an *E. coli* sensing instrument.
2. Smartphone cameras can measure fluorescence and trace it back to quantify the amount of *E. coli* in the colony-forming unit (CFU).
3. The Surface Plasmon Resonance has sufficient detection limit to quantify *E. coli* in low units that conform to food safety quality.

1.4 Research scope

This research applied engineering, biochemistry, and microorganism knowledge to quantify the quantity of *E. coli* by measuring the fluorescence product (4MU) from the GUD enzyme secreted by *E. coli* with its substrate MUG. A gelatin microfluidic with MUG suspended was used as a sensing instrument, which is green technology, cost-effective, and

low-cost, applied with simple instruments such as a smartphone camera for recording the fluorescence signals. The SPR simulation with effective refractive index theory that uses electromagnetic wave phenomena can be used as the *E. coli* detection and find the detection limit.

1.5 Research plan

Table 1.2 Present research plan within 2 years

Operation plan	Research progress / 2 months											
	2	4	6	8	10	12	14	16	18	20	22	24
1. Research preparation and literature review.												
2. Establish a research plan and research procedure.												
3. Experimental calibration and create a calibration curve.												
4. Cultivate *E. coli* and find the relationship of the colony-forming unit.												
5. Preparing a microfluidic channel and study characteristics.												
6. Applied microfluidics with *E. coli* detection.												
7. Record and evaluate the experimental simulate data.												
8. SPR *E. coli* detection												
9. Prepare a paper manuscript and publish												

CHAPTER 2
RELATED THEORIES

2.1 Foodborne pathogen

2.1.1 Introduction to Foodborne pathogens

Foodborne pathogens, which generally consist of bacteria, viruses, or parasites, cause severe foodborne illnesses [26]. Foodborne illness occurs when the human host consumes food that has a foodborne pathogen and produces a toxin. The most common pathogenic bacteria are *Escherichia coli*, *Salmonella* spp., *Shigella* spp., *Staphylococcus aureus*, *etc.* It can cause symptoms mild to severe such as nausea, vomiting, diarrhea, abdominal pain, fever, insomnia, muscular pain, labour breathing, and respiratory paralysis. It has been reported that the foodborne outbreak in European Union (EU) in 2015 resulted in more than 45,000 patient sickness cases, over 3,800 hospitalizations, and 17 deaths due to the foodborne illness. The prevention and management of all emerging foodborne diseases, a global concern, need a coordinated approach from all nations and the appropriate international organizations. Even though their biology, analysis, and epidemiology are complicated, most foodborne illnesses are preventable. It is necessary to combine knowledge and abilities from several areas. To avoid food contamination on farms, during processing, in restaurants, and in homes, public health organizations, regulatory authorities, the food industry, and consumers must continuously attempt to prevent it. The number of cases of foodborne diseases might be reduced with appropriate education programs for everyone concerned [27].

2.2 *Escherichia coli*

Escherichia coli or *E. coli* is one of the most common foodborne pathogens and is generally found in the environment, foods, and intestines of mammals. *E. coli* is a Gram-negative, non-spore-forming rod; some rods have flagella while others do not (Figure 2.1). Most *E. coli* strains are harmless, but some have developed characteristics, such as the

capacity to produce toxins, that make them pathogenic to mammals. According to the pathogenic mechanism, six categories of pathogenic *E. coli* have been identified: (1) Enteropathogenic *E. coli* (EPEC); (2) Enterohemorrhagic *E. coli* (EHEC), widely known as Shiga toxin-producing *E. coli* [STEC]; (3) Enterotoxigenic *E. coli* (ETEC); (4) Enteroaggregative *E. coli* (EAggEC); (5) Enteroinvasive *E. coli* (EIEC); and (6) Attaching and Effacing *E. coli* (A/EEC) [27, 28].

Figure 2.1 Show *E. coli* gram staining observed under a microscope with a magnification of 100x [29].

According to Table 1.1, there are several techniques for *E. coli* detection, for example culturing in media culture as a traditional method, biochemical test, RT-PCR, quantum dot, Surface Plasmon Resonance, nano biosensor, or enzyme activity. Since a laboratory-based technique is typically employed for its evaluation, detecting and counting *E. coli* typically needs a long period to obtain the results. The traditional technique, culturing, requires 24-72 hours after sampling. Although more rapid methods for detecting *E. coli* in water, such as Polymerase Chain Reaction (PCR) and Enzyme-Linked Immunosorbent Assay (ELISA), have been developed, their widespread use in water quality detection is still constrained by the need to transport samples from water sources to laboratories, high costs, complicated equipment usage, and complex procedures [30].

2.3 Microfluidic channel

A Microfluidic channel is a device that manipulates and controls the small fluid of the sample. The main reason for the rapid development of microfluidic systems has been their potential for a wide range of biological applications, such as pharmaceutical and single-cell or molecular analysis. There are many applications for microfluidics, given its ability to significantly reduce sample volumes and carry out the reaction, separation, and detection quickly and sensitively at a fraction of the typical time and cost [31, 32].

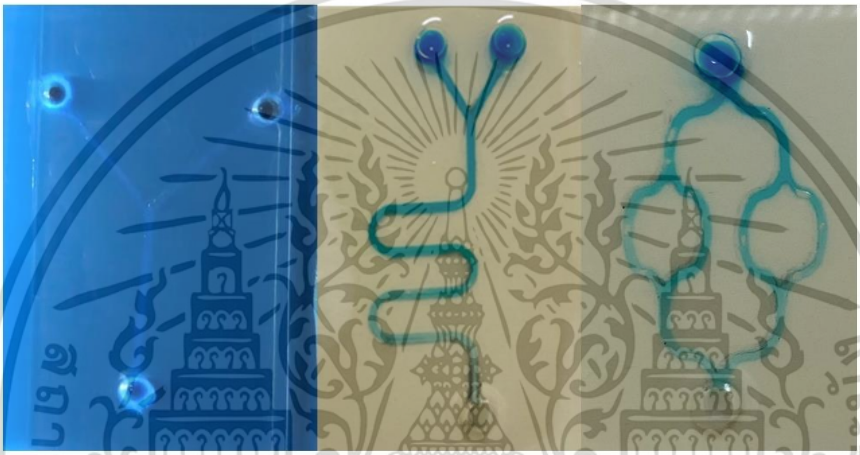

Figure 2.2 Example of the microfluidic channel

Microfluidic devices can be applied in various applications. Since the 1960s, test strips, or "lateral flow assays," have achieved wider recognition in the diagnostic industry thanks to their low-cost production of billions of units. Although in terms of the quantity of commercially available devices, this may be regarded as the most successful microfluidic platform for lab-on-a-chip applications (e.g., diabetes testing, pregnancy testing, *etc.*) [33]. It has also been reported that microfluidic can be applied for manipulating, concentrating, and separating bioparticles in biological labs, including fluorescence or magnetically activated cell sorting, centrifugation, filtration, and manipulations and separations based on electric fields [34].

For the fabrication of microfluidics, a variety of materials make an effort to achieve these characteristics, including transparency, biocompatibility, chemical compatibility with the indicated reagents, and the possibility for surface functionalization. Glass, silicon, metals, polymers, and ceramics are standard materials. Due to its easy availability, chemical

compatibility, and thermostability, silicon is among the top choices for fabricating microfluidic devices. Glass-based microfluidic can withstand chemical reactions that call for challenging circumstances, including high pressures, high temperatures, and acidic solvents, and also has excellent optical transparency, a reduced-cost material. PDMS, an elastomer with outstanding microchip fabrication properties, is one of the most significant materials for fabricating microfluidic devices. With optical transparency, gas permeability, biocompatibility, low autofluorescence, natural hydrophobicity, and high elasticity, PDMS is inexpensive, simple to mold, and suitable for prototyping. These characteristics make PDMS useful for bio-related research studies, such as longer cell cultures, cell screening, and biochemical experiments [35].

2.4 Gelatin

Gelatin is a naturally present polymer formed by the hydrolytic degradation of collagen protein obtained from animals. The primary sources of gelatin are the collagens from pigs, cows, and fish. Gelatin can be dissolved at high temperatures [36], but the structure will become gelatinous at temperatures below 35-40 °C. Additionally, the viscosity and gel strength of gelatin change with the relative molecular mass distribution, while pH, temperature, and electrolyte condition all may have an effect. The manufacturer has a critical standard for evaluating the gel strength of gelatin [37].

Figure 2.3 Shows the gelatin powder image [38]

Gelatin can be applied in many applications, such as in food industries, cosmetics, pharmaceuticals, hydrogel, scaffolds, nanoparticles, and nanofiber. Due to its ability to gel, gelatin is an essential part of the food industry in modern cuisine, for example, dessert and

canned meat, to retain lost juices. Gelatin is an excellent material for edible coating and film because of its high nutritional value and film-forming ability. Gelatin is also crucial in the medical field. It can be used as a hemostasis to prevent blood bleeding, make hydrogel, carriers for cell transplants, nanomicrosphere containers, and nanofibers. Additionally, oral gelatin consumption can enhance joint and bone health [37].

2.5 Ultraviolet

Ultraviolet (UV) is a form of electromagnetic radiation with shorter wavelengths than visible light, ranging from about 380 nm to about 10 nm. Commonly, UV radiation is divided into UVA, UVB, and UVC, which correspond to different wavelengths [39, 40].

UV radiation can be absorbed by various substances, including minerals, plants, fungi, bacteria, and organic and inorganic compounds, and emit fluorescence. The material's electrons move to a higher energy level due to absorption. Then, these electrons can decrease to a lower energy level, emitting some of the energy they had previously absorbed as visible light [41].

2.6 Logistic growth curve

It is popular to use the logistic growth curves (S-curves) model to research and predict future changes with Equation (1), as shown in Figure 2.4. It is characterized as a phenomenological description of the time behavior for quantities described using empirical time series that has been optimized. The fitting model, a logistic S-curve, is essential because it represents the natural growth pattern in the environment's interaction [42, 43].

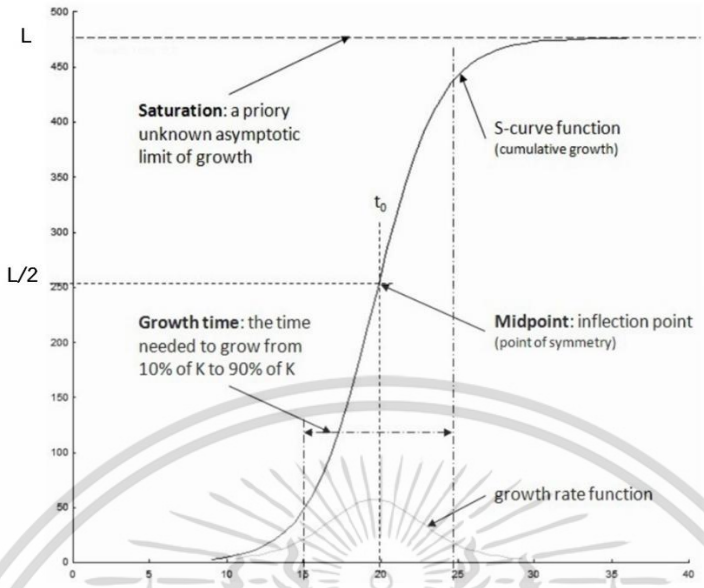

Figure 2.4 Schematic representation of a logistic S-curve with 3 parameters consisting of saturation (L), growth rate (k), and midpoint (t_0) with bell shape curve fitting as shown in Equation (1).

$$f(t) = \frac{L}{1+e^{-k(t-t_0)}} \quad (1)$$

Where L is the saturation point

k is the logistic growth rate

t_0 is the mid-point (point of symmetry)

2.7 Principle of the enzymatic reaction of GUD and MUG

To indicate *E. coli*, the enzymatic reaction of β-D-glucuronidase (GUD) enzyme was widely used as the *E. coli* biomarker. GUD enzyme activity is present in approximately 97% of *E. coli* strains, indicating the organism's presence in environmental samples, particularly water [22]. 4-methylumbelliferyl- β-D-glucuronide (MUG) was the substrate that can be hydrolyzed by GUD and get the fluorescence product called 4-methyl-umbelliferone (4MU). When 4MU is excited by a UV light source around 360 nm, the blue fluorescence will be emitted at a wavelength of around 450 nm [13, 44].

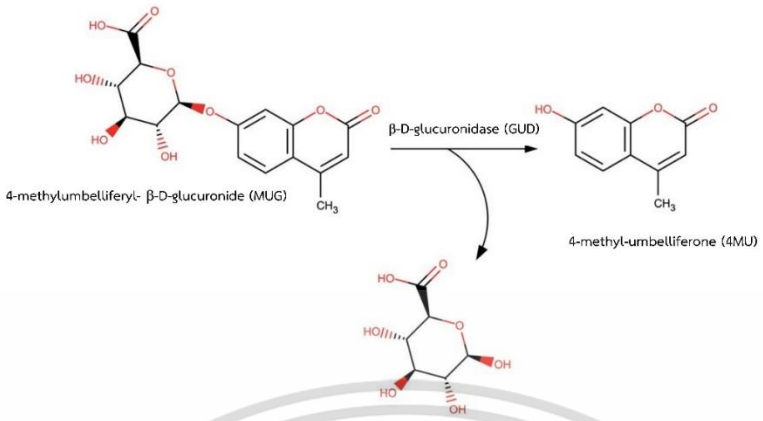

Figure 2.5 Structure of MUG and 4MU [44]

2.8 Cell culture

Cell culture is the process of growing and increasing the number of cells controllable from an animal, plant, or microorganism such as bacteria by allowing them to develop in a suitable artificial environment. Several techniques for cell culture or isolating the microorganism include a streak and spread plate [45].

2.8.1 Spread plate technique

The spread plate technique is a common counting approach to identify or count the microorganisms in a liquid sample. The technique allows you to calculate the number of bacteria colonies distributed on the plate, which will be visible and countable in the colony-forming unit (CFU) [46, 47].

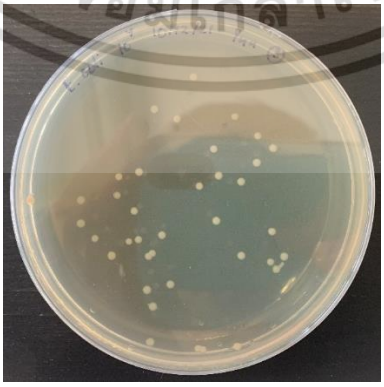

Figure 2.6 Example of the *E. coli* colony on solid media agar by spreading plate technique.

2.9 Principle of light

Light is one of the electromagnetic waves that have an extensive range. The visible light ranges from 380 nm to 770 nm and purple to red light, respectively. Since light is an electromagnetic wave, its characteristics, such as its magnetic field, electric field, wavelength, speed, refractive index, reflection, diffraction, interference, and polarization, are identical to those of an electromagnetic wave [48].

2.9.1 Magnetic field and electric field

Magnetic and electric fields which parts of light that are perpendicular to the electromagnetic wave's direction of motion and each other. Figure 2.7 depicts how the right-hand rule raw can determine the direction of the relationship between the magnetic field and the electric field [49, 50].

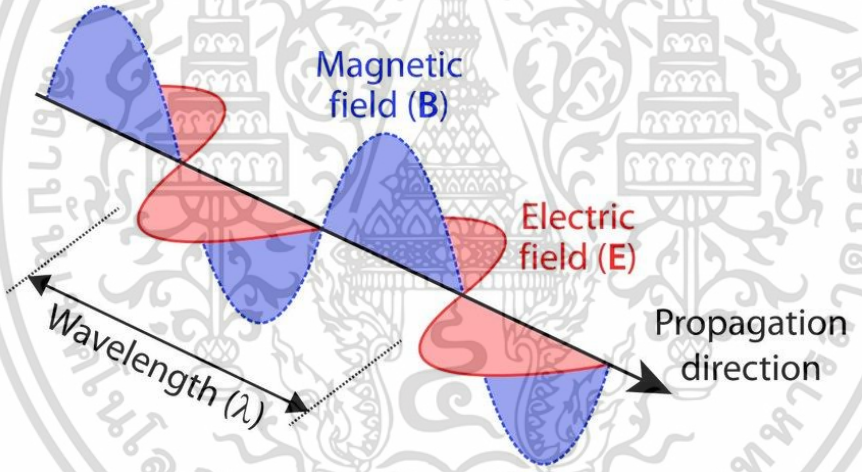

Figure 2.7 Show the relationship and the direction of the magnetic field and electric field [51].

2.9.2 Refractive index

The Refractive index is defined as the ratio of the velocity of light divided by its velocity as expressed in Equation (2); however, the light's wavelength and speed depend on the material through which it travels [52]. The refractive index can change inside the same medium if the electromagnetic wave frequency varies.

$$n = \frac{c}{v} = \frac{\lambda}{\lambda_0} \quad (2)$$

Where n is the refractive index of the medium

c is the velocity of light in the vacuum

v is the velocity

λ_0 is the light speed in the free space

2.9.3 Reflection

One of the characteristics of light is reflection, which occurs when incident light travels and contacts certain surfaces that do not absorb the energy of the light. The law of reflection, depicted in Figure 2.8 and represented in Equation 3, indicates that this light will reflect off of that surface and change direction, making the reflection angle equal to the incident angle but in the opposite direction [53].

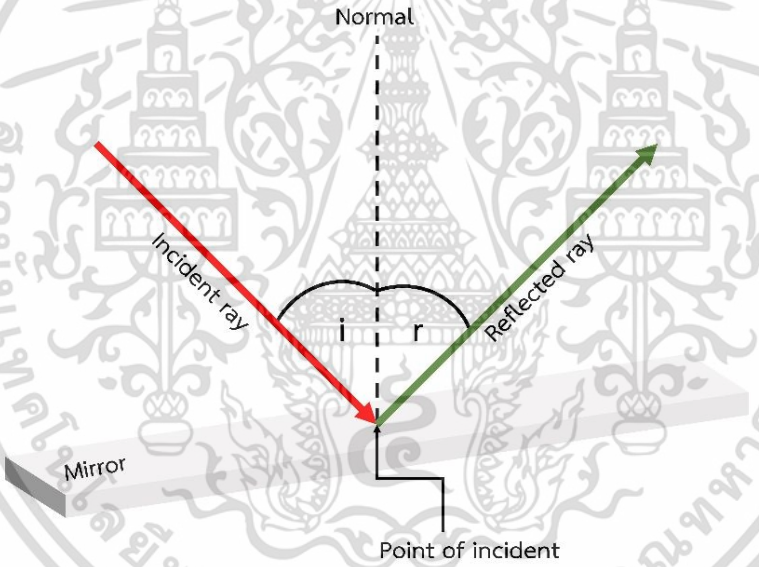

Figure 2.8 Shows the schematic of the incident ray and reflected ray by the law of reflection.

$$\theta_i = \theta_r \tag{3}$$

Where θ_i is the angle of incidence in a unit of radian or degree

θ_r is the angle of reflection in a unit of radian or degree

2.9.4 Refraction

Refraction is the term for bending light from its incidence direction as it passes through transparent media with a different refractive index (it also occurs with sound, water, and other waves). Figure 2.9 shows Snell's law of the refractive of light and is expressed in Equation (4). Additionally, this characteristic allows individuals to utilize magnifying glasses, lenses, and prisms and to visualize the rainbow [54].

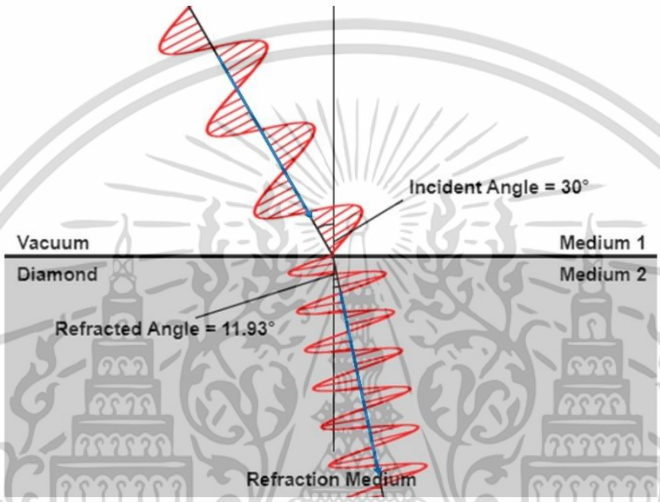

Figure 2.9 Shows the schematic of the refraction of light between vacuum (n=0) and diamond (n=2.417) with an incident angle equal to 30 degrees [55].

$$n_1 \sin(\theta_1) = n_2 \sin(\theta_2) \quad (4)$$

Where θ_1 is the angle of incidence in a unit of radian or degree

θ_2 is the angle of refraction in a unit of radian or degree

n_1 is the refractive index of the medium where light is incident

n_2 is the refractive index of the medium where light is reflected

2.9.5 Polarization

The polarized light employed in SPR-based sensors has specified the direction of an electric field. There are two different polarization properties: the first is the change in transmittance and reflectance between P and S polarization, and the second is the change in phase difference between P and S polarization (Figure 2.10). According to the direction of the electric field, the polarization can also be divided into three types (1) linear polarization,

which is utilized in SPR sensors, (2) circular polarization, and (3) elliptical polarization [56, 57].

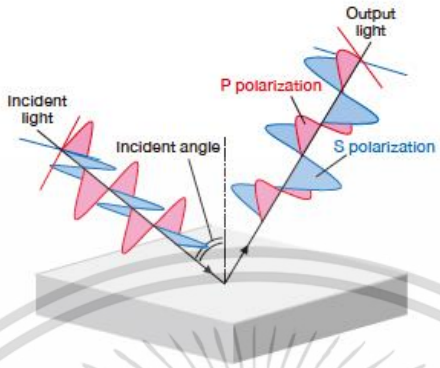

Figure 2.10 Shows the direction of electric field p-polarization (red-line) and s-polarization (blue-line) [56]

2.10 Polarization and incident plane

The direction of light polarization affects both the surface plasmon resonance and evanescent wave properties. P-polarization and s-polarization are the two main polarization types identified through studies in the field of electromagnetics.

1. TM (Transverse magnetic mode) or called P (parallel) -polarization

A light wave is considered in TM-polarization when the electric field direction is parallel to the incidence plane. Additionally, in isotropic media, the magnetic field is always perpendicular to the electric field. As shown in Figure 2.11, this property causes the magnetic field to be transverse and perpendicular to the incident plane [58].

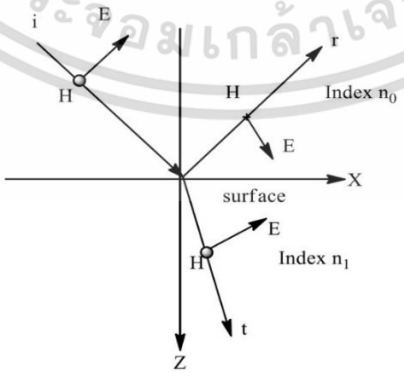

Figure 2.11 Shows the direction of the electric (E) field that is parallel to the incident plane in the TM-polarization and the direction of the magnetic field (H) [58].

2. TE (Transverse electric mode) or called S (perpendicular) -polarization

A light wave that is TE-polarization has an electric field direction that is perpendicular to the incidence plane. Figure 2.12 shows how the magnetic field exists parallel to the plane of incidence because it is always perpendicular to the electric field in isotropic mediums [58].

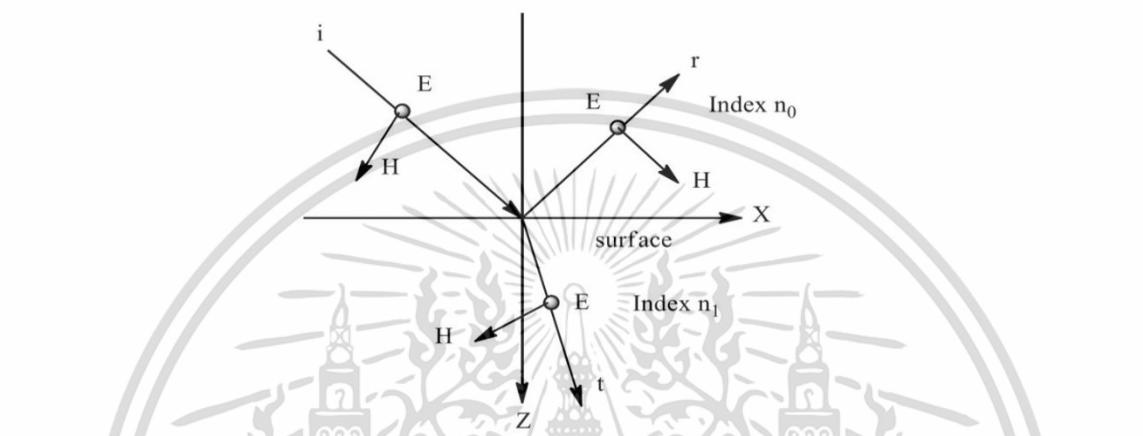

Figure 2.12 Shows the direction of the magnetic field (H) and the direction of the electric field (E) that is perpendicular to the incident plane in the TE-polarization [58].

2.11 Surface Plasmon Resonance

Surface plasmon resonance (SPR) is a limited electromagnetic wave phenomenon that occurs on the interface between the dielectric material and the noble metal surface. The refractive index, absorbance, and fluorescence properties of analyte molecules can be measured in SPR sensors to determine the desired quantity [59, 60]. The first SPR sensor application occurred in 1982, while Nylander and Liedberg employed it for gas detection and biosensing [61]. Then noble metals that are usually used in SPR sensors are gold (Au), silver (Ag), and Copper (Cu). However, gold is typically used as a noble metal in biological and biomedical studies because it provides an applied quantitative of coupling wavelengths and angles for surface plasmon resonance. Gold is also chemically stable and biocompatible, making it suitable for biological and biomedical applications [62].

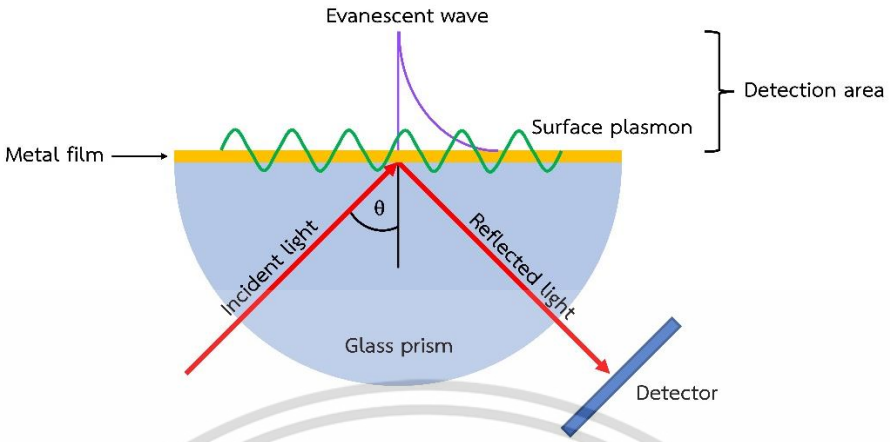

Figure 2.13 Shows the principle of the SPR sensor that detects the change in the refractive index

The photons will illuminate the noble metal film layer in the sensor as they travel through the optical source and hit the SPR-based sensor. Surface plasmons are the oscillations of the noble metal interface and the excited electron that occurs when photons hit the noble metal layer (Figure 2.13). As a result, the electric field will be created at the interface instead of the hitting site. Then, the surface plasmons will generate an evanescent wave, a similar field extending on both sides of the noble metal layer [63]. The refractive index of the sensing area for the light, which is perceived as reflected due to a different velocity in a different medium, is one of the characteristics of the medium that this travelling electric field also depends on. Additionally, as the different medium compositions, the velocity of the plasmons changes, affecting the angle of incident light at which the resonance occurs.

CHAPTER 3

METHODOLOGY

This chapter describes the materials and methodology of this research. As previously mentioned, the enzyme GUD produced by *E. coli* reacts with its substrate MUG to produce the fluorescent product of the catalytic reaction known as 4MU. This enzyme activity technique widely uses GUD as a biomarker for detecting *E. coli.* The experimental procedure performed the enzymatic reaction under the nutrient agar and then applied MUG-suspended gelatin-based microfluidics to quantify the amount of *E. coli* in CFU units. The SPR simulation will be proposed later with practical refractive index theory for *E. coli* detection.

3.1 Enzyme-substrate reaction experiment on MUG-suspended nutrient agar with cultured *E. coli*

This experiment aimed to determine if the enzyme GUD produced by *E. coli* can diffuse through agar. This substance is likely to gelatinize and then bind with MUG substrate suspended in nutrient agar, whether it can sufficiently bond with its substrate or not. So, the nutrient agar was prepared by mixing 0.3% Yeast Extract (Himedia), 0.5% Peptone (Himedia), 0.5% NaCl (Ajex), and 1.5% Agar (Hemidia) sterilized by autoclave at 100 °C mixing with 125 μM of MUG (Sigma). Due to the substrate not being tolerant at high temperatures, MUG sterilized was added later after sterilizing the nutrient agar using a filter. The *E. coli* (TISTR 527, ATCC 11775), purchased from the Thailand Institute of Scientific and Technological Research (TISTR), was cultured in liquid media with the incubator at 150 rpm for 24 hours at 37 °C. After that, *E. coli* was cultured by streak and spread plate technique and incubated in the incubator at 30 °C for 24 hours.

3.2 Fluorescence and catalytic reaction calibration by using a fluorescence spectrophotometer setup

In this experiment, the experimental setup was the fluorescence spectrophotometer with significant components consisting of a smartphone camera (iPhone X.S. Max), UV light source, 4 side-transparent plastic cuvette (VWR International Ltd.), and additional optical filter as shown in Figure 3.1. All the below experiments in this section 3.2 will be tested under this setup.

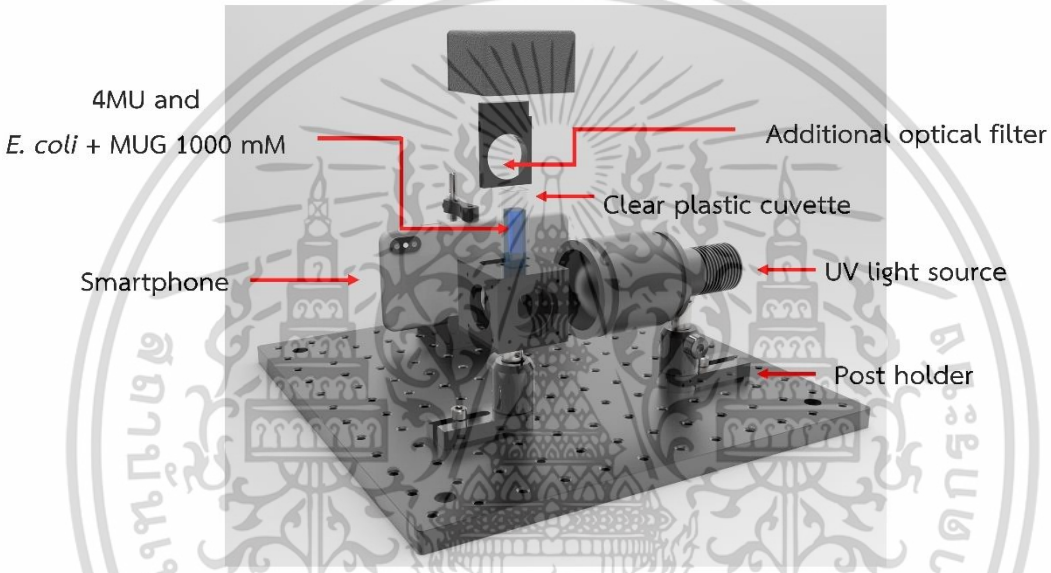

Figure 3.1 Fluorescence spectrometer setup

In order to eliminate UV background light, transparent acrylic was used as an additional optical filter, as depicted in Figure 3.2. The transmittance of this filter was evaluated using a spectrophotometer (model V-5100/UV5100, METASH). According to Figure 3.2, an optical filter can filter all UV light wavelengths under 360 nm and allow the above wavelength to pass through, including a 450 nm wavelength of 4MU. So, it was efficient to use as an optical filter in this experiment.

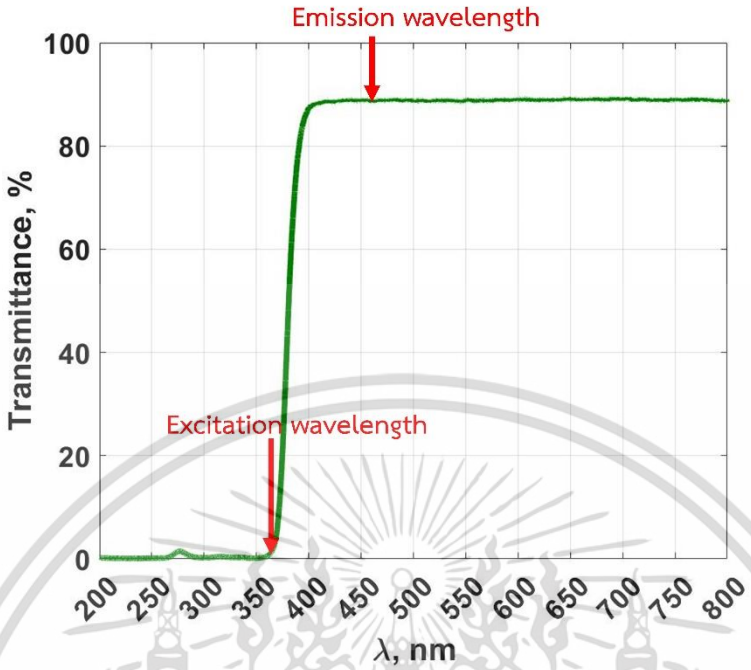

Figure 3.2 Spectral transmittance of additional optical filter measured by using the spectrophotometer

3.2.1 Calibration for the 4MU intensity using fluorescence spectrophotometer experimental setup

This experiment was set for calibrating the fluorescence intensity of 4MU as a baseline trend. The iPhone camera was compared to find the proper setting of ISO, used for controlling the amount of light by the sensor's sensitivity, for collecting a 4MU fluorescence intensity signal. Due to the light intensity, the maximum number in MATLAB is 256, so the highest concentration of 4MU was used to find the proper ISO that got the fluorescence intensity lower than 256. Here, 1 ml of 4MU (Aldrich) was prepared for 8 diluted concentrations varying from 0.5 μM to 500 μM diluted with methanol. The fluorescence spectrophotometer setup shown in Figure 3.1 was applied to evaluate each 4MU concentration, and each fluorescence light emission was recorded 3 times. After converting the fluorescent signal in MATLAB, plot the relationship between the 4MU concentration and fluorescence intensity signal.

3.2.2 *E. coli* colony counting

The colony counting technique calculated the number of bacteria in CFU/ml unit by cultivating on solid media and counting the appeared colony on it. So, I have performed the *E. coli* colony counting for calculated own *E. coli* concentration converting equation. The procedure is to cultivate *E. coli* in a conical flask at 30 °C for 24 hours, as shown in Figure 3.3. Then diluted *E. coli* at a dilution factor of 10^6, $10^{6.5}$, 10^7, $10^{7.5}$, and 10^8 times and cultivated in solid media agar repeated 3 times of each concentration with 100 µl. The number of *E. coli* in CFU/ml units, which corresponds to the dilution factor, was calculated using the colony counting technique after incubating at 37 °C for 24 hours.

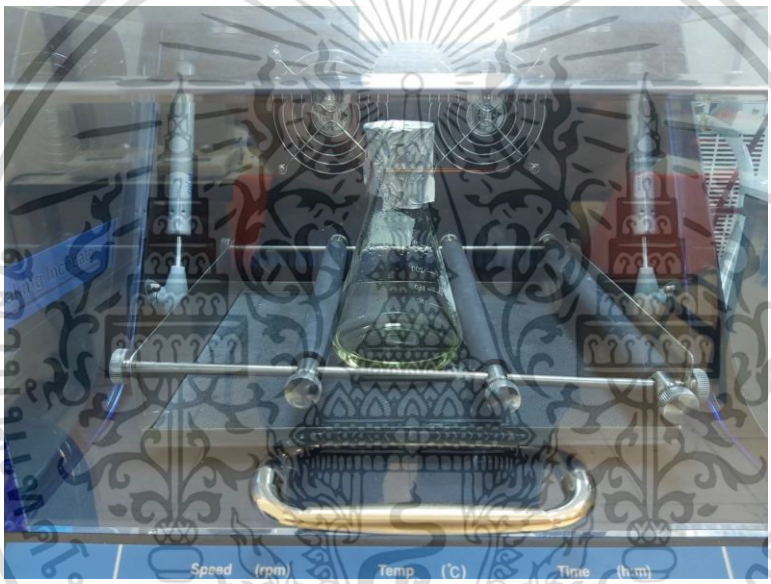

Figure 3.3 *E. coli* cultivated in a shaking incubator at 30 °C for 24 hours

3.2.3 Calibration for the fluorescence intensity from different *E. coli* concentration

The methods for calibrating the fluorescence of varied *E. coli* concentrations were identical to those for calibrating with 4MU. *E. coli* was grown in a conical flask for 24 hours before being diluted at concentrations ranging from 2 to 500 times, or 6.79×10^6 CFU/ml, 3.53×10^7 CFU/ml, 7.17×10^7 CFU/ml, 3.73×10^8 CFU/ml, 7.58×10^8 CFU/ml, 1.94×10^9 CFU/ml, and 3.94×10^9 CFU/ml, respectively. The equation from the section on the *E. coli* colony counting experiment, which will be presented afterwards in the result section, was used to

compute the various *E. coli* concentrations in CFU/ml units. 500 ml of 1000 μM of MUG was mixed with 500 ml of each *E. coli* concentration under a transparent plastic cuvette. The fluorescence intensity of the reaction was continuously measured every 15 minutes for 4 hours with the experimental setup depicted in Figure 3.1. The data recorded from the smartphone camera were calculated in MATLAB and plotted the relationship between fluorescence intensity signal and time. This experiment aimed to ensure that the fluorescence signal was visible to the naked eye.

3.3 MUG-suspended gelatin-based microfluidic channel preparation

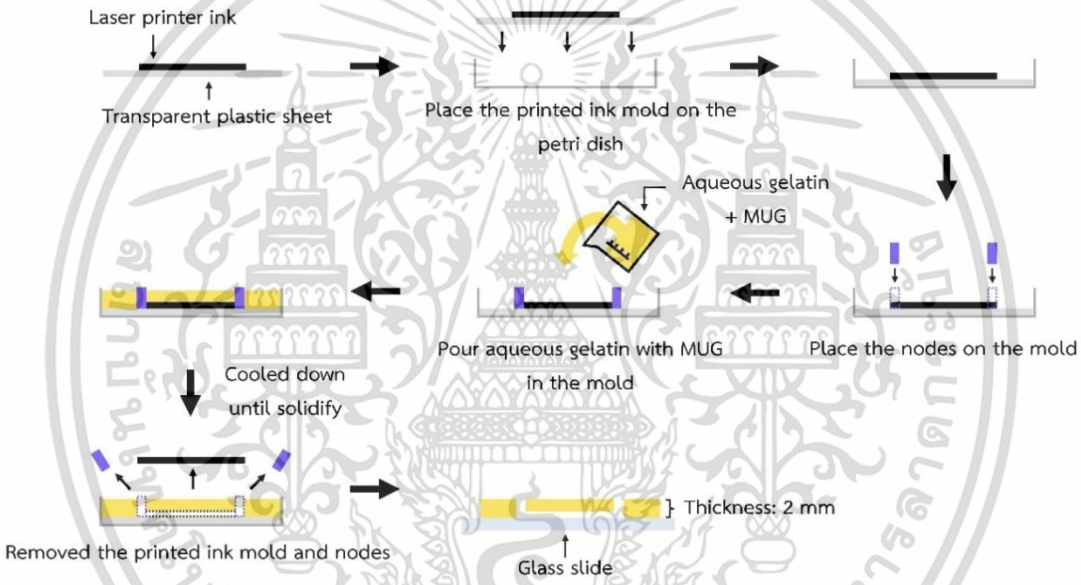

Figure 3.4 Gelatin-based microfluidic with MUG suspended fabrication diagram

My recently published paper Microfluidic Channel from Gelatin Using Laser Printer [64], proposed procedures for fabricating microfluidic channels from gelatin using a laser printer. The 3-point, or 1 mm, width and 3 cm in length straight-line channel pattern was designed in Microsoft PowerPoint. The pattern was then printed 30 times on a transparent plastic sheet (Hi-jet laser) by a laser printer (Canon LBP-6030) to increase the laser printer ink thickness as the height of the channel. Gelatin powder (Gelita, Thailand) was dissolved in warm distilled water at a ratio of 1 g : 3 ml and the powder was thoroughly stirred until it was completely dissolved. The MUG substrate (Sigma) at 500 μM was then added to the gelatin solution, bringing the total concentration of the solution to 250 μM. Pour the

warmed gelatin aqueous over the printed ink mold once it has cooled in the refrigerator, enabling the gelatin to solidify into a gel, as shown in the fabrication diagram depicted in Figure 3.4.

3.4 Experimental setup and measure the enzyme activity from *E. coli* under MUG-based gelatin microfluidic

The MUG-suspended fluidic channel from the previous section was applied to detect *E. coli*. The material and procedures of the microfluidic fabrication method described in section 3.3 were used to prepare the 6 microfluidic channels. The experimental setup was as shown in Figure 3.5 with components consisting of (1) iPhone X.S. max, (2) monopod, (3) UV light source, and (4) 6 microfluidic channels.

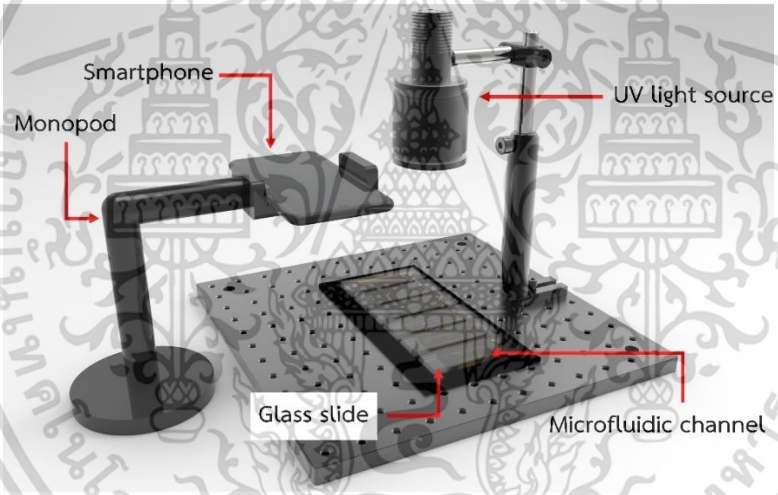

Figure 3.5 Experimental setup for measuring the enzyme activity from the different concentrations of *E. coli* under gelatin microfluidic channel

6 samples were employed to test separately consisting of:

1. Distilled water as a negative control
2. Enzyme GUD at 1700 U/ml as a positive control
3. Cultivated *E. coli* at 3.94×10^9 CFU/ml
4. Cultivated *E. coli* at 3.53×10^7 CFU/ml
5. Cultivated *E. coli* at 3.16×10^5 CFU/ml
6. Cultivated *E. coli* at 2.83×10^3 CFU/ml

The equation calibrated from the previous *E. coli* colony counting experiment was used to determine all *E. coli* CFU/ml units, which were presented in the results section. In order to evaluate the 6 samples, 0.3 ml of each sample was then fed through the separated 6 different straight-line microfluidics at the inlet node of the microfluidic channels, depicted in Figure 3.6.

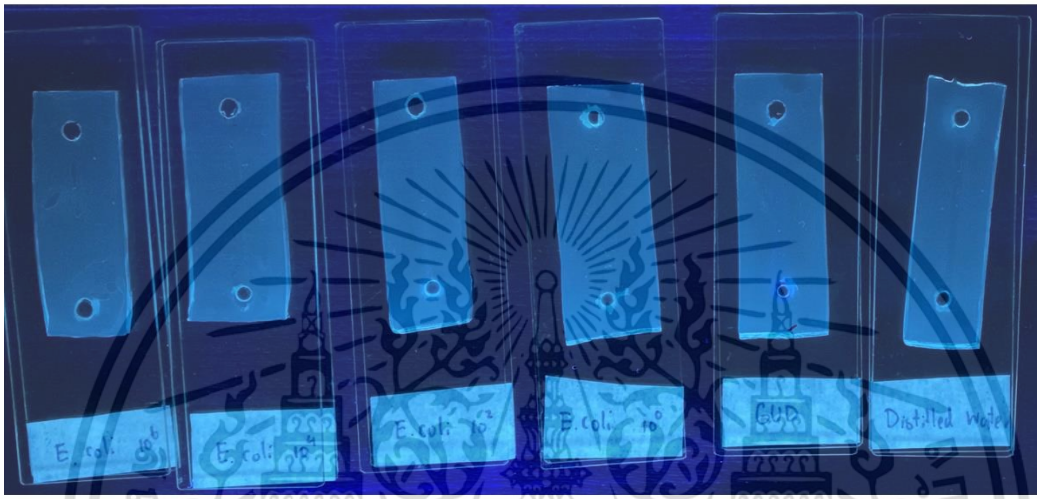

Figure 3.6 6 samples were fed through MUG suspended gelatin channel observed under Figure 3.5 experimental setup

The blue fluorescence light stimulated under the UV light source, as in the experimental setup shown in Figure 3.5, was then measured and compared using a smartphone camera to record a time-lapse video of the fluorescence emission for 5 hours within the gelatin channels. In MATLAB, the blue light intensities recorded for each video frame along each gelatin channel were subtracted from the red and green color intensities recorded in the red-green-blue (RGB) format to analyze the video.

3.5 Surface Plasmon Resonance with Effective refractive index theory

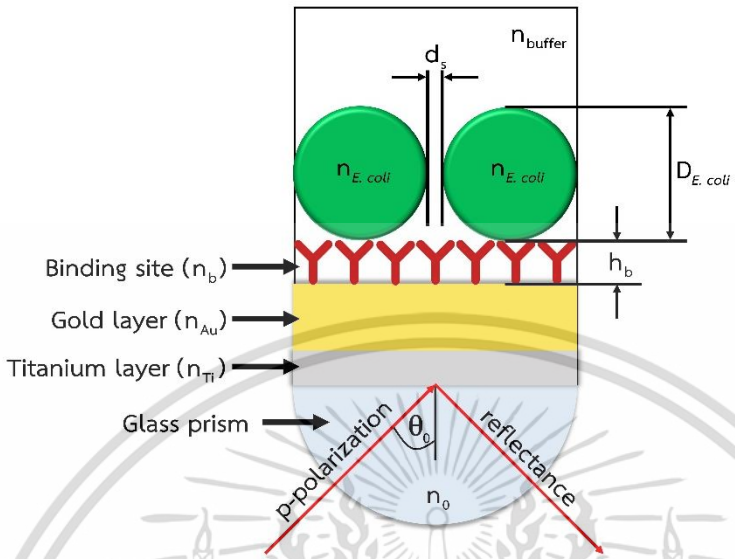

Figure 3.7 *E. coli* with the Kretschmann configuration

In this research section, I have reported the simulation and modelling of the effect of *E. coli* detection by using the SPR sensor with detection limit and the sensitivity of the SPR. To propose the sensitivity and detection limit for quantitative *E. coli* detection SPR model. A Kretschmann configuration was made up of a 50 nm uniform plasmonic gold sensor with a gold refractive index of n_{Au} reported by Johnson and Christy in 1972 [65] coated on a BK7 glass substrate with a glass refractive index of 1.51 and illuminated by a p-polarized optical configurable laser source at incident angle 0. Figure 3.7 shows a titanium adhesion layer with a 5 nm thickness between the glass substrate and the gold layer. This layer has a refractive index of n_{Ti} [65]. *E. coli* can bind specifically to the gold sensor surface due to a binding site and molecules with the refractive index n_b and thickness h_b shown in Figure 3.7. The surrounding buffer solution has a refractive index of 1.336 [66], while *E. coli* has a refractive index of 1.384 [67], with an approximate diameter of 1 μm and a length of 2 μm [68].

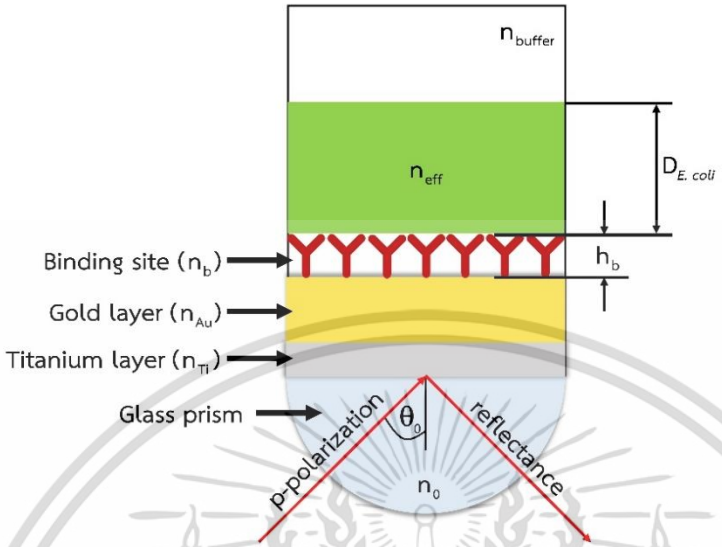

Figure 3.8 Configuration of the effective refractive index

E. coli colony modelling is restricted by the orientation of each *E. coli* on the binding site and random arrangement, along with the colony's measurement in the CFU/ml unit. Nevertheless, as the *E. coli* binding is distributed on the sensor surface density and not the volume density, this unit does not accurately represent the number of *E. coli* present on the sensor surface. In order to depict *E. coli*'s random orientation and distribution, optical modelling needs a complicated calculation technique.

In this study, I have proposed an effective refractive index model [69] to calculate the *E. coli* colony as a uniform layer with an effective refractive index n_{eff} as indicated in Equation (5) and a thickness of 1 m equivalent to the average diameter of *E. coli* $D_{E.\ coli}$ [68].

$$n_{eff} = \frac{\pi r_{E.\ coli}^2 n_{E.\ coli} + (D_{E.\ coli}(d_s + D_{E.\ coli}) - \pi r_{E.\ coli}^2) n_{buffer}}{D_{E.\ coli}(d_s + D_{E.\ coli})} \quad (5)$$

Where $n_{E.\ coli}$ is the refractive index of *E. coli*

d_s is the cell density level

$r_{E.\ coli}$ is the *E. coli* cross-sectional plane's radius, which is equal to $\frac{D_{E.\ coli}}{2}$

The *E. coli* surface density can be calculated from Equation (5).

$$S_{E.coli\ density} = \frac{1}{L_{E.\ coli}(d_s + D_{E.\ coli})} \quad (6)$$

Where $L_{E.\ coli}$ is the *E. coli* cell body length, which is approximately 2 mm [68].

3.6 Simulation methodology and detection limit

Fresnel equations and the transfer matrix method were used to model the reflectance spectra of the p-polarization for *E. coli* measurements using the Kretschmann configuration and the effective index theory shown in Figure 3.7. The modelling software was developed and performed using parallel processing in MATLAB 2021a.

For comparison with experimental results published in the article, the plasmonic coupling wavelength's movement in nm over the CFU/ml unit is used to compute the sensitivity or S. The CFU/ml threshold that corresponds to the typical bulk refractive index of 10^{-5} refractive index units (RIU) for intensity detection is known as the limit of detection (LoD) [70].

CHAPTER 4

EXPERIMENTAL RESULTS AND DISCUSSION

4.1 Enzyme-substrate reaction experiment on MUG-suspended nutrient agar with cultured *E. coli*

Using the streak and spread plate procedures, *E. coli* was cultured on nutrient agar mixed with MUG. The result is shown in Figures 4.1b and 4.1d, observed under a UV light source found that in the nutrient agar plate suspended with MUG occur, the fluorescence emitted around the *E. coli* colonies. On the other hand, as depicted in Figures 4.1a and 4.1c for the spreading and streaking techniques, the nutrient agar without the MUG enzyme resulted in no fluorescence around the colonies. Therefore, these investigations demonstrated that the GUD enzyme is released extracellularly by *E. coli*. This enzyme can be employed as a biomarker for identifying *E. coli* by measuring the blue fluorescence of the 4MU products produced by the enzymatic reaction of GUD and MUG. As demonstrated by these experiments, it is also established that GUD was secreted extracellularly by *E. coli* and can diffuse through an agar bond with a substrate and cause a reaction.

Figure 4.1 Nutrient agar with (a) without MUG suspended in nutrient agar; and (b) mixed with MUG which *E. coli* was cultivated by spread plate technique; Nutrient agar with (c) without MUG suspended in nutrient agar; and (d) mixed with MUG which *E. coli* was cultivated by streak plate technique;

4.2 Fluorescence and catalytic reaction calibration by using a fluorescence spectrophotometer setup

4.2.1 Relationship of fluorescence intensity and different 4MU concentrations

This experiment aimed to demonstrate the correlation between the concentration of 4MU and the intensity of the blue fluorescence emission. The 4MU 500 μM was used for calibrating the smartphone camera ISO setting by measuring the fluorescence intensity and was then calculated in MATLAB. The explanation is that since I utilized the highest concentration of 4MU in this experiment, 500 μM, the fluorescence intensity in this experiment should be at its highest. Figure 4.2 demonstrates the outcome, which indicated that the ISO was adjusted from 25, 40, 100, 200, 500, 1000, and 2000. The top line should be equal to or less than 256 since, as described in section 3.2.1, the maximum light intensity in MATLAB was 256. The fluorescence intensity index of 500 μM of 4MU is shown in Figure 4.3. The ISO 500, 1000, and 2000 indexes were more significant than 256 in every cuvette area, while this ISO was higher than 200. To summarize, ISO 200 worked perfectly to measure smartphones' fluorescence intensity signal in this experiment.

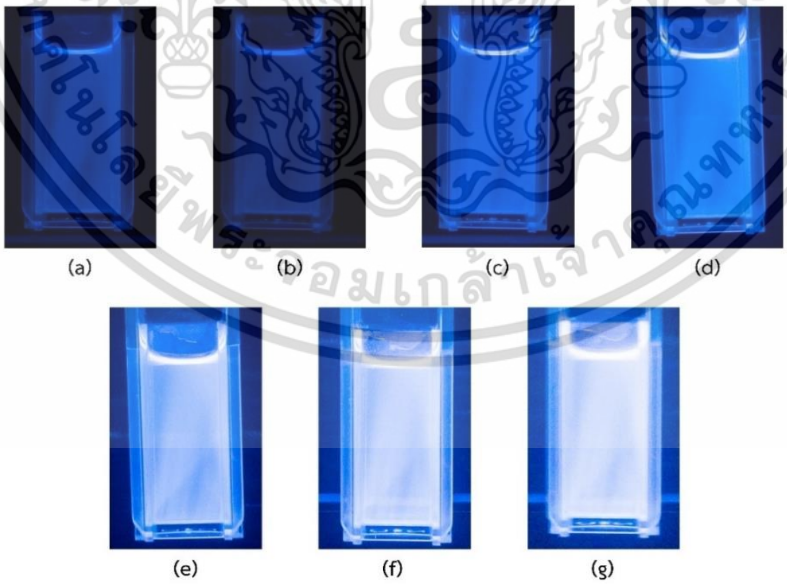

Figure 4.2 The fluorescence of 4MU concentration 500 μM recorded by smartphone camera at (a) ISO 25; (b) ISO 40; (c) ISO 100; (d) ISO 200; (e) ISO 500; (f) ISO 1000; and (g) ISO 2000

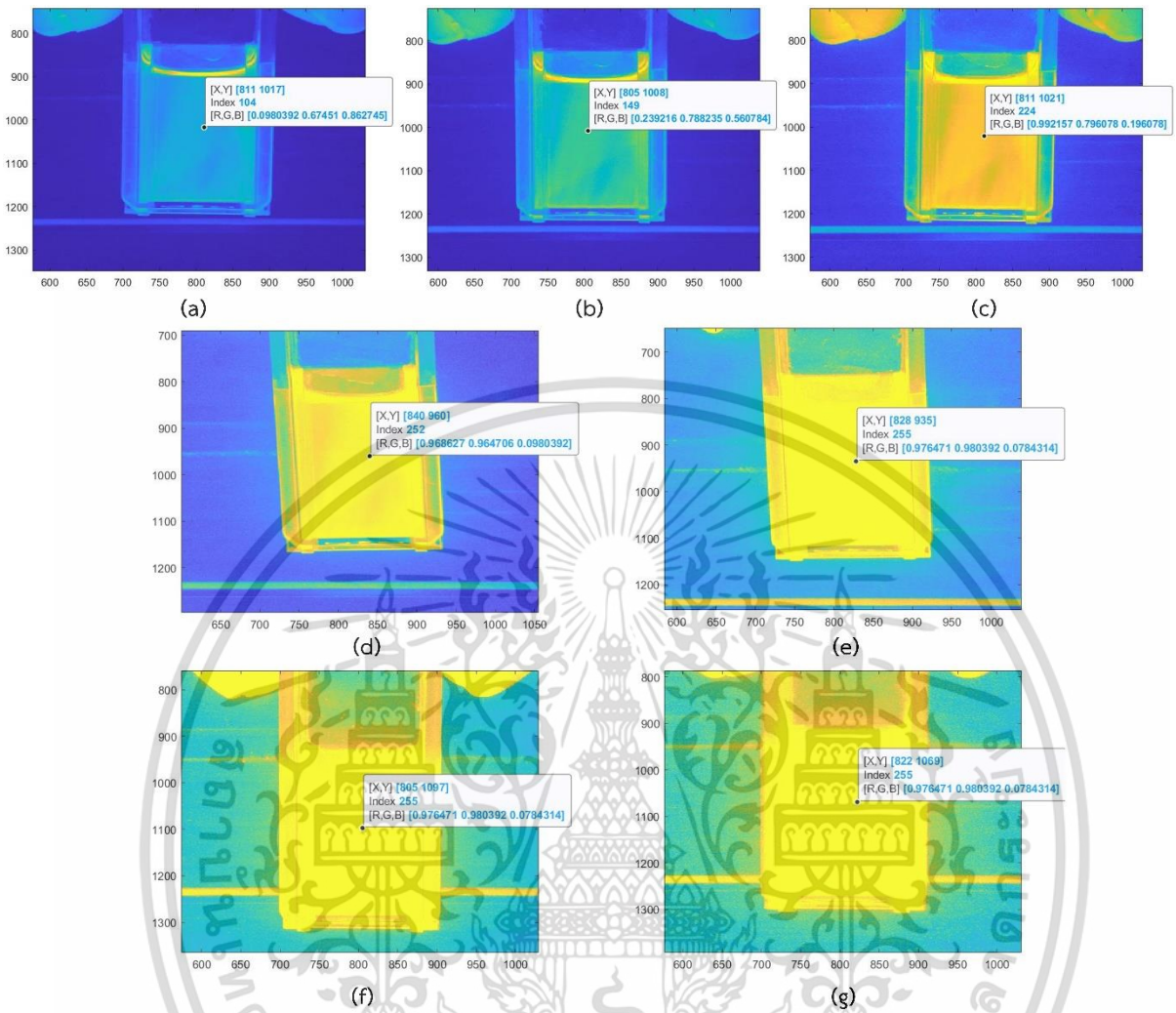

Figure 4.3 4MU fluorescence intensity measured index under MATLAB range from (a) ISO 25; (b) ISO 40; (c) ISO 100; (d) ISO 200; (e) ISO 500; (f) ISO 1000; and (g) ISO 2000

Then the 4MU concentration varying from 0.5 μM to 500 μM diluted in methanol was recorded fluorescence intensity and calculated in MATLAB. The relationship between normalized fluorescence response and 4MU concentration is shown in Figure 4.4. Each concentration was measured repeatedly 3 times and shown the error bar as ± one standard deviation of the three measurements. The result has shown that the fluorescence intensity signal was increased linearly as a proportion of the 4MU concentration's logarithmic scale. This linear curve fitting relationship had a coefficient of determination R^2 of 0.90, as expressed in Equation (7).

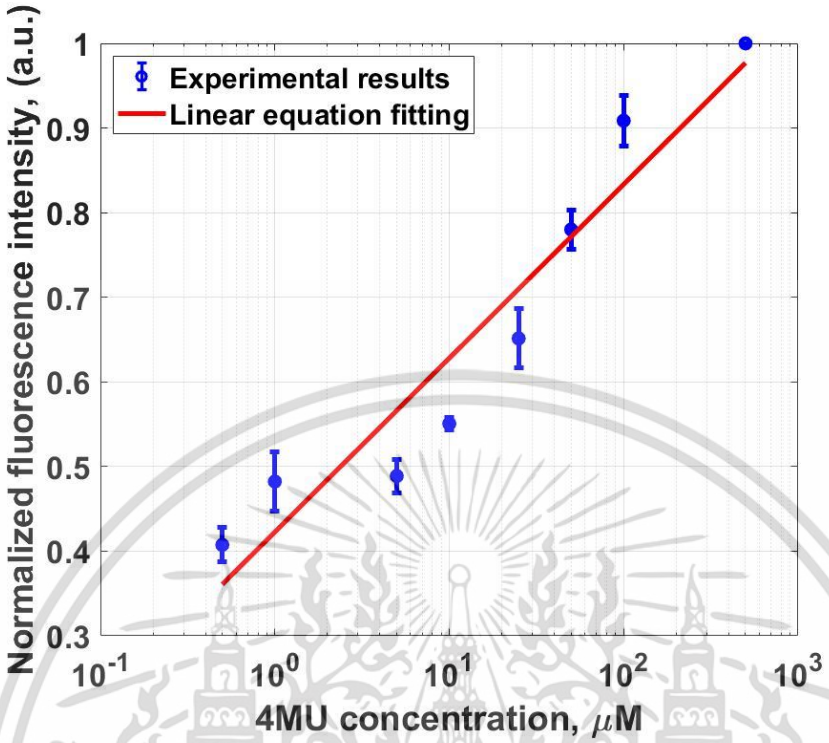

Figure 4.4 Show the relationship between the fluorescence signal of 4MU concentration between 0.5 μM to 500 μM, along with the linear curve fitting equation

$$f_s([4MU]) = 0.345\log([4MU]) + 0.017 \quad (7)$$

Where f_s is the normalized fluorescence signal in an arbitrary unit (a.u.)

[4MU] is the 4MU concentration in μM.

It has been demonstrated that the fluorescence signal is linearly proportional to the concentration on the logarithmic scale. Note that the purpose of the experiment was to show a relationship between the 4MU concentration and the intensity of the blue fluorescence. Experimental and measurement errors could be the cause of the variation from the straight line. Due to the previously noted measurement inaccuracy, the relationship in Equation (7) was not used to calibrate the sensor in the following sections.

4.2.2 *E. coli* colony counting

E. coli was cultured in solid nutrient agar for colony counting with 5 dilution times corresponding to 10^6, $10^{6.5}$, 10^7, $10^{7.5}$, and 10^8 times by spread plate technique. Each concentration was done 3 times, and the colony counting result is shown in Figure 4.5.

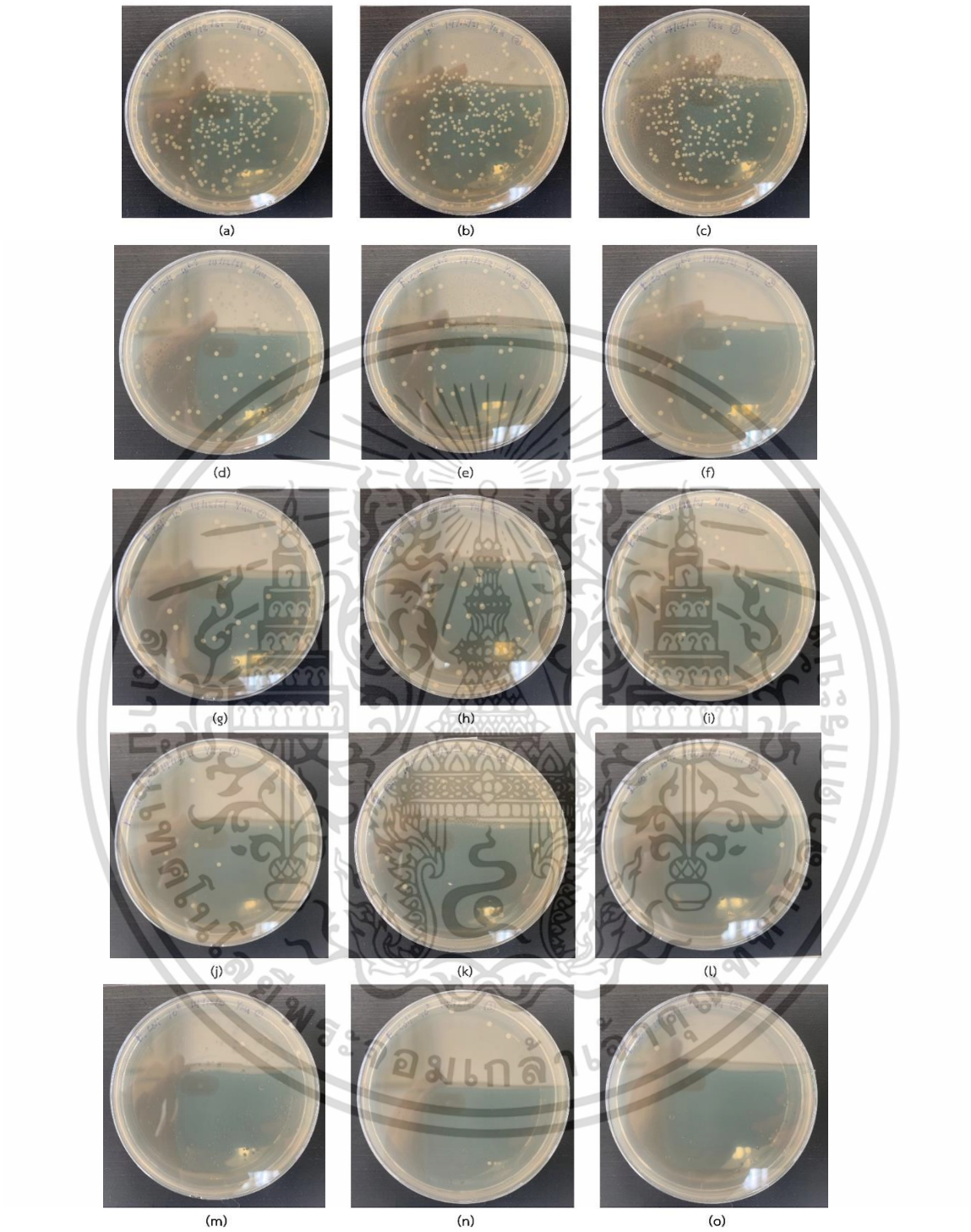

Figure 4.5 Show the *E. coli* spread plate cultivated for colony counting with concentration at dilution time corresponding to (a) Plate1; (b) Plate2; and (c) Plate3 of 10^{6} times, (d) Plate1; (e) Plate2; and (f) Plate3 of $10^{6.5}$ times, (g) Plate1; (h) Plate2; and (i) Plate3 of 10^{7}, (j) Plate1; (k) Plate2; and (l) Plate3of $10^{7.5}$, and (m) Plate1; (n) Plate2; and (o) Plate3of 10^{8} times

Then the results of the colony counting were summarized and plotted against the dilution factor and the CFU/ml *E. coli* concentration on a logarithmic scale, as depicted in Figure 4.6. The number of times the initial *E. coli* colony is diluted is referred to in this experiment as the dilution factor. In the logarithmic scale, a dilution factor of 2 indicates a 10^2- or 100-times dilution of the initial *E. coli* concentration. This was acknowledged that the relationship between bacterial colonies and their dilution factor is linear on the logarithmic scale. The colony counting equation was shown in Equation (8) with an R^2 of 0.98.

$$\log(CFU/ml) = -1.024\log(Dilution\ factor) + 9.5955 \quad (8)$$

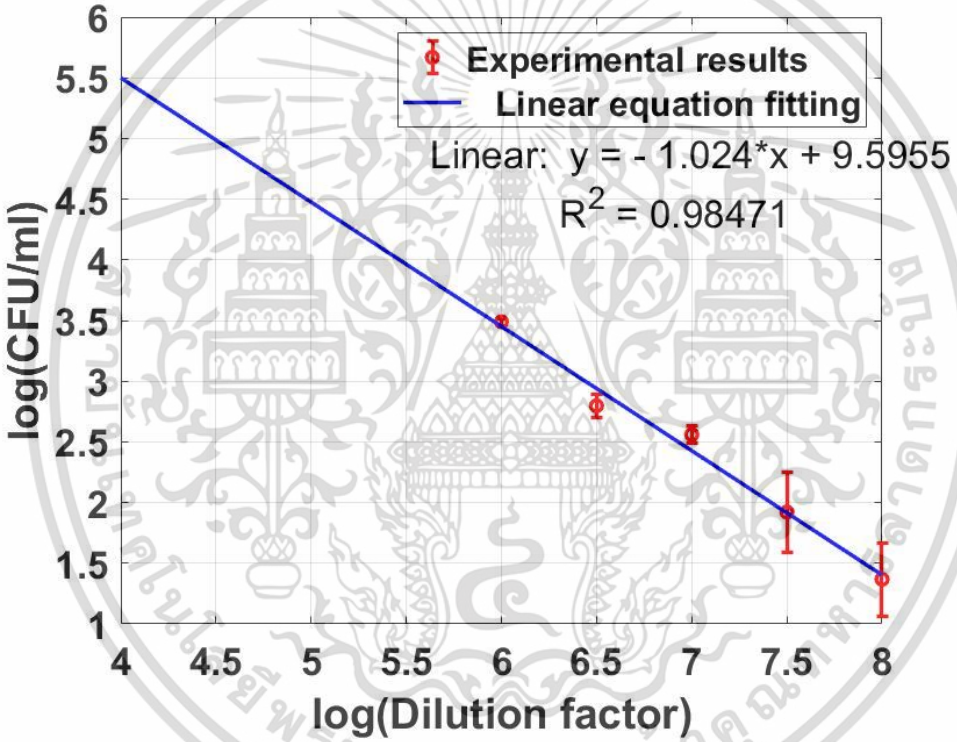

Figure 4.6 Relationship between *E. coli* concentration in CFU/ml unit and dilution factor in logarithmic scale and linear curve fitting.

4.2.3 Relationship between the fluorescence intensity from different *E. coli* concentration and time

Here, the *E. coli* 7 different concentrations, 6.79×10^6 CFU/ml, 3.53×10^7 CFU/ml, 7.17×10^7 CFU/ml, 3.73×10^8 CFU/ml, 7.58×10^8 CFU/ml, 1.94×10^9 CFU/ml, and 3.94×10^9 CFU/ml, while CFU/ml was calculated from Equation (6), was mixed with 1000 μM of MUG in

cuvette as using the experimental setup in Figure 3.1. Each concentration recorded fluorescence intensity continuously every 15 minutes for 4 hours, resulting in the relationship shown in Figure 4.7.

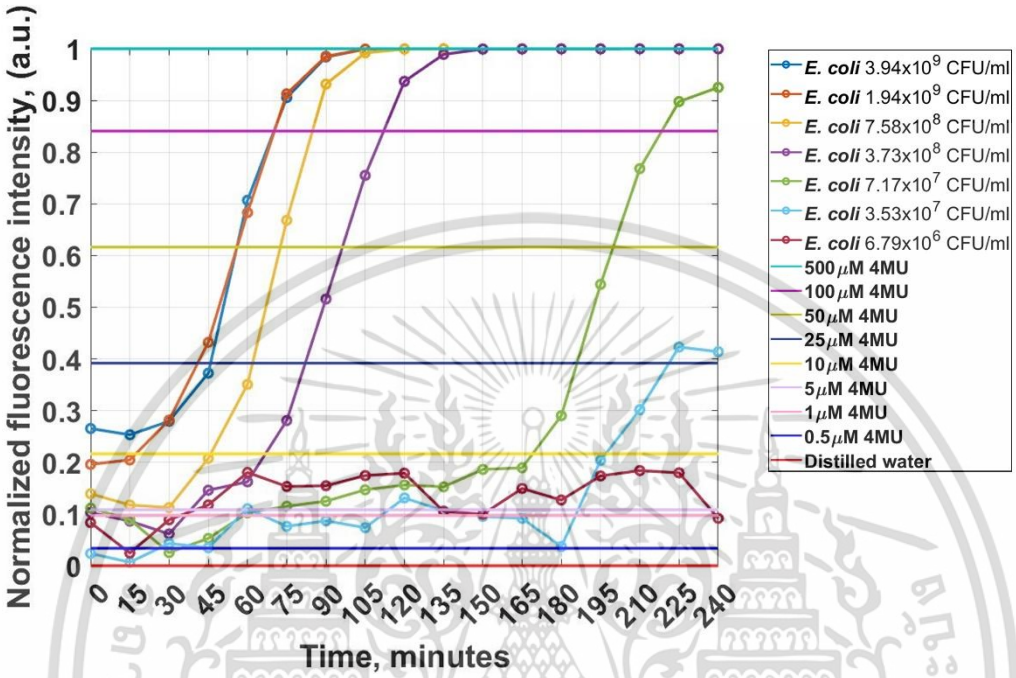

Figure 4.7 Normalized fluorescence intensity signal of each *E. coli* 7 concentration measured every 15 minutes for 4 hours.

Following that, a logistic growth model [71] with an R^2 of 0.99 was utilized to curve-fit the normalized fluorescence signals. This model is depicted in Figure 4.8 and is expressed in Equation (8). All *E. coli* concentrations showed increased fluorescence intensity over time with varying time delays. The delay time constant β, which is proportional to the amount of time needed for the GUD and the MUG to form the enzyme-substrate complex, is the time it takes for the fluorescence intensity to reach 0.5 on the normalized fluorescence intensity scale.

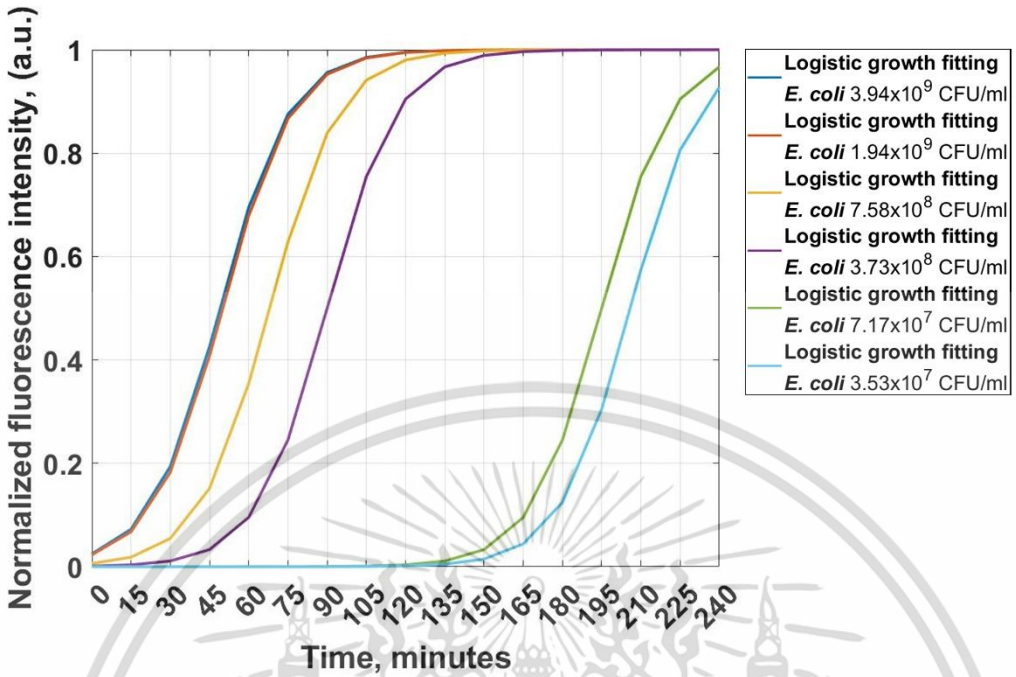

Figure 4.8 Logistic growth curve fitting of fluorescence intensity signal in Figure 4.7 with Equation (9)

$$f_s(t,[E.coli]) = \frac{1}{1+e^{-0.075(t-\beta([E.coli])}} \quad (9)$$

Where f_s is the normalized fluorescence signal in an arbitrary unit (a.u.)

t is time in minute

[*E. coli*] is *E. coli* concentration

β is the model delay time constant given by

$$\beta(Dilution\ factor) = 88.741 \times \log(Dilution factor) + 25.378 \quad (10)$$

Which can be related to the linear fitting colony counting equation in Figure 4.6 and Equation (8)

$$\beta([E.coli]) = -86.661 \times \log\left(\frac{CFU}{ml}\right) + 856.93 \quad (11)$$

The fluorescence intensity signal of distilled water showed zero intensity level, while *E. coli* showed an S-shaped curve. It is known that the logistic growth curve can be used to explain why the colony growth of microorganisms, like *E. coli*, exhibits an S-shaped curve because there is a lack of nutrition and available space for forming colonies [72].

4.3 MUG-suspended gelatin-based microfluidic channel preparation

Here, a straightforward method for creating microfluidic channels using a laser printer that was created and just recently reported [64] was used in this study. A straight-line pattern with a 1 mm width and 3 cm length was created and printed 30 times on the transparent plastic sheet. Vernier calliper and microscope measured the deposited ink layer on the plastic film cut in the cross-sectional plane. For the 30 times of printing, the printed ink had a height of 190 μm and a width of 1.78 mm, as shown in Figure 4.9. As you can see, the channel's width widened by 1.78. The printer's paper feeding mechanism error and the plastic sheet's thermal expansion were caused for the expanded channel. To create six microfluidic channels in section 3.4, the printed pattern depicted in Figure 4.9 was adopted and used once again. Note that the ink layer on plastic film can reuse as the mold for fabricating a gelatin-based microfluidic channel.

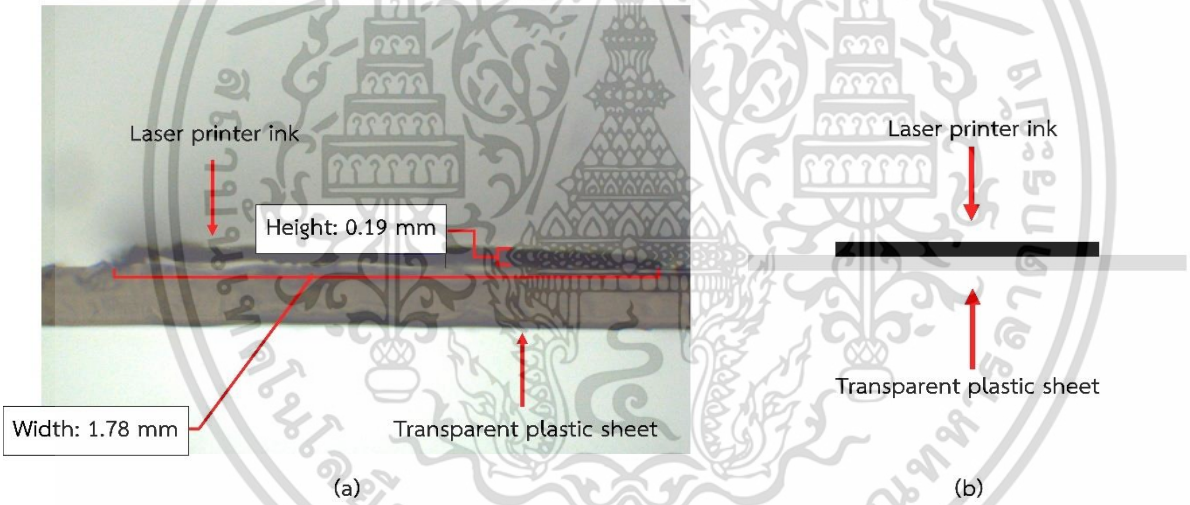

Figure 4.9 (a) Cross-sectional of ink layer on plastic film under the microscope; (b) Schematic explanation of Figure 4.9 (a)

The spectrophotometer was used to prepare and characterize the 2 mm thick gelatin film, and Figure 4.10 displays its optical transmittance and the spectral sensitivity of the iPhone camera [73]. The UV filtering property of the gelatin and the smartphone camera sensitivity allows the transmittance at higher than 455 nm to pass through it but filter out all wavelengths below 400 nm.

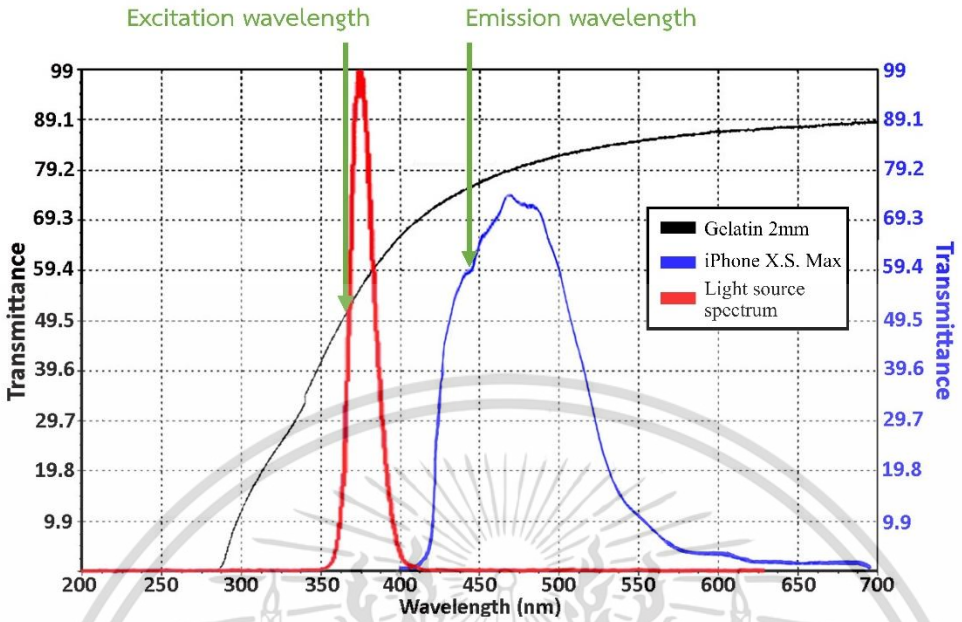

Figure 4.10 The UV light source spectrum with enzyme-substrate emission spectrum, the optical spectrum of the 2 mm gelatin fluidic, and iPhone's camera spectral sensitivity

Even though the 50% UV transmittance of the gelatin film is insufficient to block the excitation wavelength of 355 nm, as measured and illustrated in Figure 4.10, this wavelength is essential for fluorescence excitation. The fact that the incident light went through the gelatin film twice must be underlined. To clarify, the UV light source's excitation wavelength passed through the gelatin film and excited the blue fluorescence in the channels with 50% of its optical power first. The power of the blue fluorescence would be lowered if the UV absorption inside the gelatin film were too high. After that, the excitation wavelength was reflected off the gelatin film's opposite way. The excitation wavelength's optical intensity was further decreased by at least a factor of 4 as the reflected light propagated to the front surface. Recall that at the interfaces, optical power was also lost.

However, because the 4MU fluorescence emission was excited inside the channels, the wavelength of the 4MU fluorescence emission, mainly based around 460 nm, only passed through the gelatin film once with a higher transmittance of 75%, as shown in Figure 4.10. Moreover, the high fluorescence quantum yield of 70% [74] of 4MU leads to a stronger fluorescence signal than the UV background. Additionally, the iPhone camera's spectral responsiveness can filter out the background and only capture the blue fluorescence light, as shown in Figure 4.10. Consequently, the excitation and emission wavelengths of the 4MU

are suitable with these optical filtering effects and the optical transmittance [20], enabling straightforward instrumentation without the need for an additional optical UV filter for the proposed enzymatic *E. coli* detection method.

4.4 Results of the enzymatic reaction from *E. coli* under MUG-based gelatin microfluidic and quantification

This experiment demonstrates that the microfluidic channel can carry out the identical enzymatic reaction covered in chapter 4.2.3 while requiring a smaller sample volume and expressing quantitative *E. coli* detection instrumentation. So, the experiment was created to determine whether the enzyme GUD secreted by *E. coli* in liquid culture could produce the blue fluorescence of 4MU. The first step involved creating the six straight-line gelatin fluidic channels using the procedures outlined in section 3.3. 0.3 ml of 6 samples consisting of distilled water, 1700 U/ml of GUD, *E. coli* 4 different concentrations were fed separately in each channel. After that, blue fluorescence was stimulated using a UV light source. The smartphone camera and the built-in video recording app were used to record the fluorescence emission of the six channels at 30 frames per second for 5 hours.

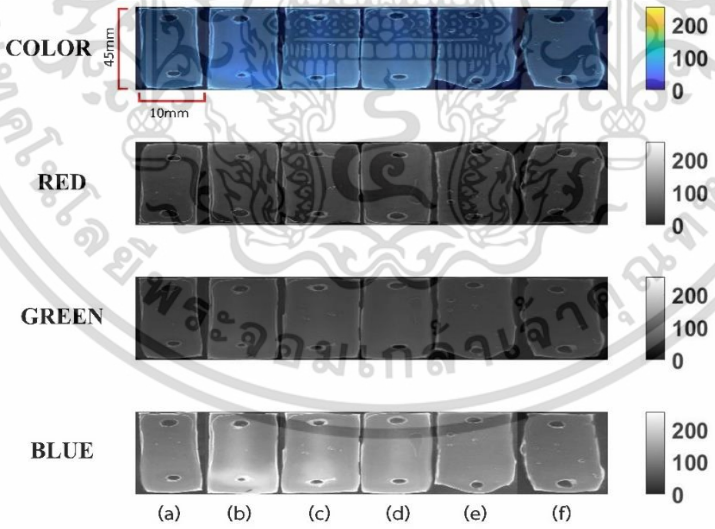

Figure 4.11 Show fluorescence response at the experiment's 5th hour (a) distilled water; (b) 1700 U/ml of the GUD enzyme; (c) Cultured *E. coli* 3.94×10^9 CFU/ml; (d) Cultured *E. coli* 3.53×10^7 CFU/ml; (e) Cultured *E. coli* 3.16×10^5 CFU/ml; and (f) Cultured *E. coli* 2.83×10^3 CFU/ml.

After a 5-hour experiment, 3 color channels (red, green, and blue) were visible in the recorded video file, as depicted in Figure 4.11. The red, green, and blue pixels in the second, third, and fourth rows of Figure 4.11 are also depicted independently from the other two colors. Since 0.3 ml of distilled water was fed into the first channel in Figure 1.11a, no fluorescence light appeared during the experiment. As a positive control experiment, 0.3 ml of the GUD enzyme at 1700 U/ml was fed into the second channel in Figure 4.11b. As stated in section 4.1, the nutrient agar control experiment also demonstrated the emission of blue fluorescence light. 3.94×10^9 CFU/ml of the grown *E. coli* were added to 0.3 ml of the third channel in Figure 4.11c and the presence of blue fluorescence light after 2 hours.

Similarly to the third channel, the fourth to sixth channels likewise displayed blue fluorescence in the microfluidic channels, specifically for blue pixels, as depicted in Figures 4.11d to 4.11f. As seen in the second and third rows of Figure 4.11 compared to the fourth row, there was no fluorescence emission recorded in the red and green color camera pixels. Although there was no strong fluorescence signal apparent to the human eye in the pictures of Figures 4.11e and 4.11f, it will be demonstrated later that the fluorescence signals are there and significantly more robust than the background noise.

There was no glare light from other sources accessing the container since the experiment was performed in a closed container, dark room as the setup was shown in Figure 3.5, containing only the UV light source that was centered at 365 nm, as described and depicted in Figure 4.10. It is critical to note that smartphones typically come with artificial intelligence (AI) based camera software to improve an image, which is the primary distinction between scientific and smartphone cameras. In contrast to the blue pixels, the red and green pixels in Figure 4.11 show a strong-intensity backdrop with no fluorescence light visible inside the microfluidic channels. The 3 colors were offset by the built-in AI software, which caused the intense backdrop. Several research studies have discussed the problem of utilizing an iPhone as an optical detector [75, 76]. In order to calibrate the intensity baseline to zero and normalize the highest intensity level to one for comparisons, the blue pixel intensities were subtracted by their offset background level.

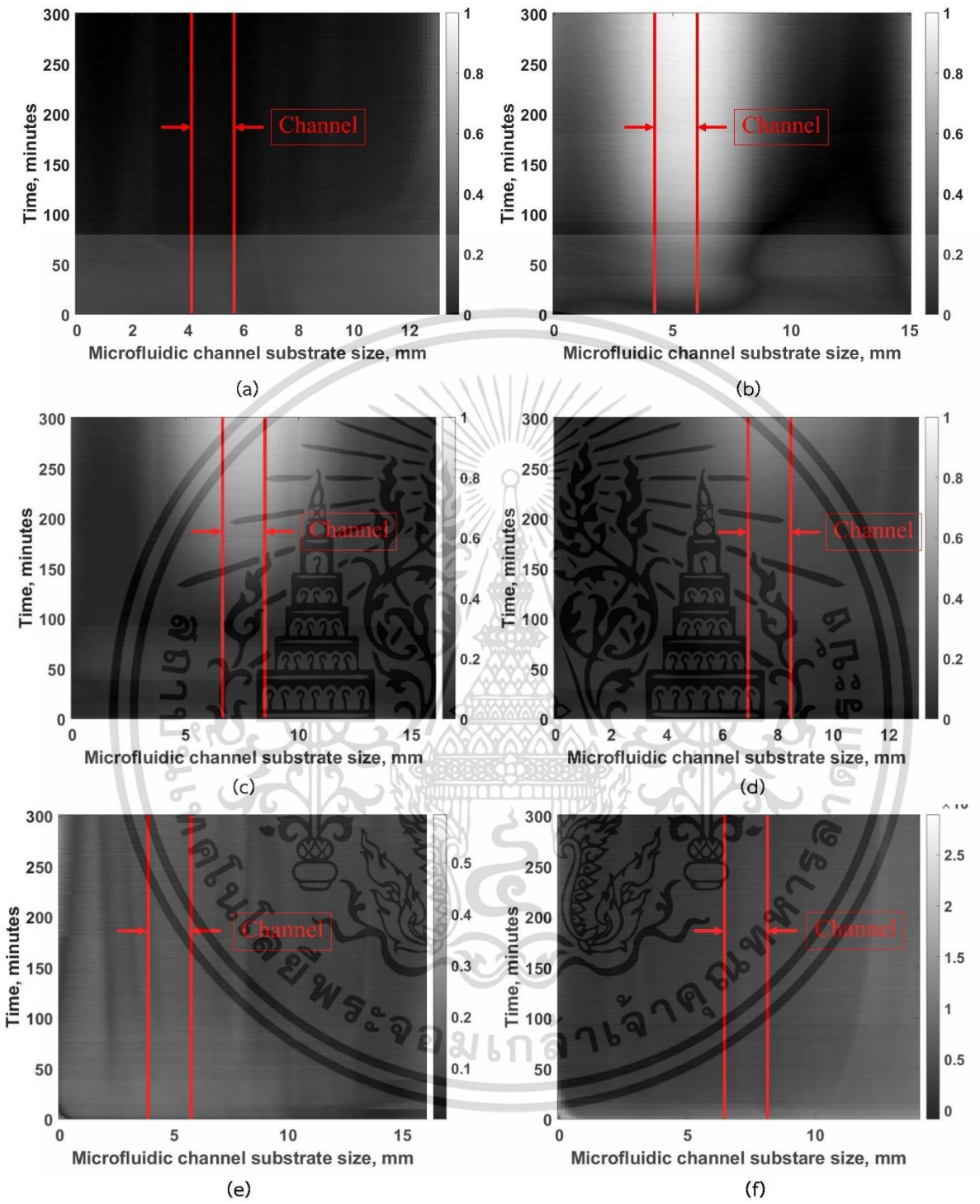

Figure 4.12 Time series data of the fluorescence response extracted from video-timelapse recorded from 0 minutes to 300 minutes for (a) distilled water; (b) 1700 U/ml of the GUD enzyme; (c) Cultured *E. coli* at 3.94x109 CFU/ml; (d) Cultured *E. coli* at 3.53x107 CFU/ml; (e) Cultured *E. coli* at 3.16x105 CFU/ml; and (f) Cultured *E. coli* at 2.83x103 CFU/m

From the first minute to the 300th minute or 5 hours of the experiment, for each of the 6 fluidic channels, Figure 4.12 shows the blue fluorescence light intensity profiles extracted from the blue pixels of the video-timelapse file. As depicted by the red lines in Figure 4.12, 6-line scans were performed here to locate the 1 mm wide channel in the middle of each fluidic channel. There was no fluorescence light inside or outside the gelatin fluidic for the distilled water sample, as depicted in Figure 4.12a. The time series data for the GUD enzyme at 1700 U/ml are presented in Figure 4.12b. The time series data for the cultivated *E. coli* at 3.94x10^{9} CFU/ml and 3.53x10^{7} CFU/ml, respectively, are shown in Figures 4.12c and 4.12d. The gelatin fluidic channel had no fluorescence light at the start of the experiment. It took at least 2 hours for the enzyme GUD secreted from *E. coli* to diffuse into the MUG-suspended gelatin channel, forming the 4MU product and emitting the blue fluorescence light. Due to the diffusion process, the blue fluorescence light emission region grew during the experiment. Compared to the 1700 U/ml case, the fluorescence signal intensity of *E. coli* was weaker. The fluorescence intensities of the lowest two *E. coli* concentrations, 3.16x10^{5} CFU/ml, and 2.83x10^{3}, will be discussed and shown later o be significantly higher than the gelatin background region and the distilled water baseline, even though they are not visible when plotted on the normalized intensity from 0 to 1 in time series data as shown in Figure 4.12e and 4.12f.

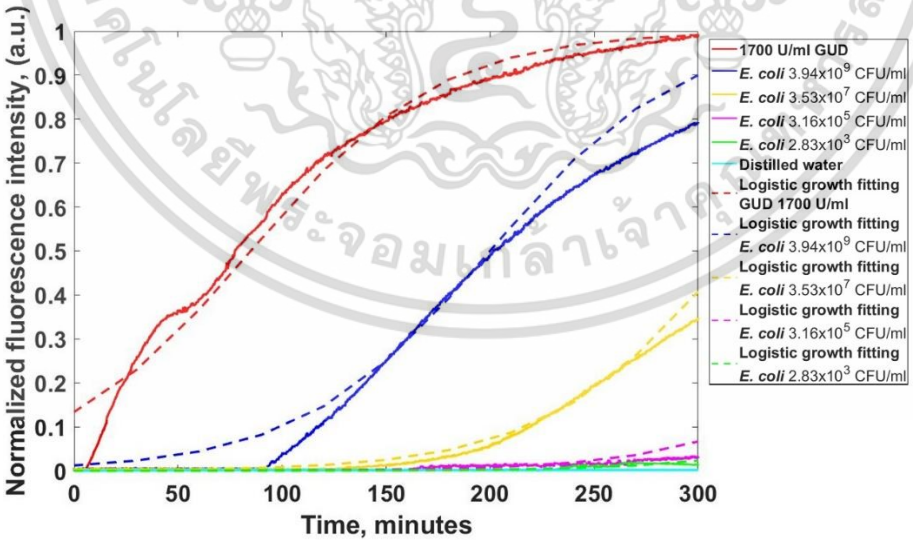

Figure 4.13 The normalized fluorescence intensities of the 6 microfluidic channels, as depicted by normalized line scan time-series data of the fluorescence responses (continuous lines) and logistic growth models (dashed lines)

The 6 channels' time-series data are displayed in Figure 4.13, along with 200 camera frame averages that total the intensities inside each red line, as shown in Figure 4.12. The measurement noise was reduced by using the averaging approach. Later in the following topic , it will describe and discuss how the average camera frames affected the results. As shown in Figure 4.12, The equilibrium of enzyme GUD at 1700 U/ml was used to normalize the total light intensity with the other data. The experiment data reported in Figure 4.13 (continuous line) were fitted curves using the logistic growth model (dashed line) described in section 4.2.3. This logistic growth equation, which has an average coefficient of determination R^2 of 0.96, is defined in Equation (12).

$$f_s(t,[E.coli]) = \frac{1}{1+e^{-0.022(t-\beta([E.coli])}} \quad (12)$$

Where the model time delay β is given by

$$\beta(Dilution\ factor) = 88.741 \times \log(Dilutionfactor) + 25.378 \quad (13)$$

Which can be related to the linear fitting colony counting equation in Figure 4.6 and Equation (8)

$$\beta([E.coli]) = -44.582 \times \log\left(\frac{CFU}{ml}\right) + 642.59 \quad (14)$$

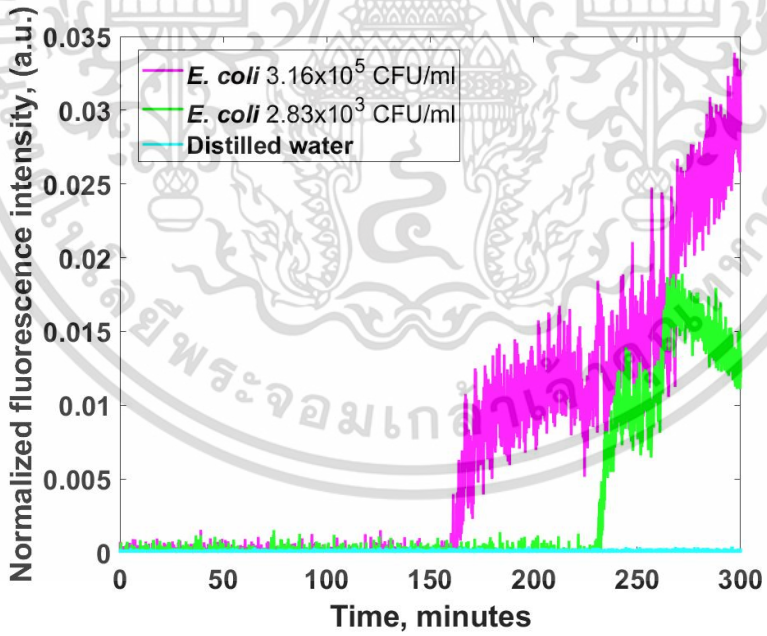

Figure 4.14 Shows the experimental signal zooming results for the concentrations of $3.16x10^5$ CFU/ml, $2.83x10^3$ CFU/ml *E. coli*, and distilled water.

The experimental results for the *E. coli* concentrations of 3.16×10^5 CFU/ml and 2.83×10^3 CFU/ml compared to distilled water are shown in Figure 4.14 on a zoomed scale from 0 to 0.035. The experiment's lowest *E. coli* concentration, 2.83×10^3 CFU/ml, had a fluorescence signal strength substantially more robust than the distilled water case's baseline intensity signal. The sensor's detection limit will be analyzed and discussed later on in the following topic.

4.5 Analysis of the detection limit of the sensing instrument

Equation (11) was expanded in this section to examine the proposed methodology's detection limit. Figure 4.15 shows the fluorescence intensity output for a range of *E. coli* concentrations, from 2 CFU/ml to 4×10^9 CFU/ml, and a range of measurement periods, from 1 hour to 5 hours. It is generally known that averaging the images throughout several frames can improve the detection limit in optical sensing [77, 78]. Of course, it thus the cost of measurement time or sensor readout effectively averages out the measurement noise at the time. As determined from the experimental results in Figure 4.12 for the distilled water case, the horizontal lines in Figure 4.15 show the measurement standard deviations (σ) for varying the number of averaging frames, from none to 25,600 frames.

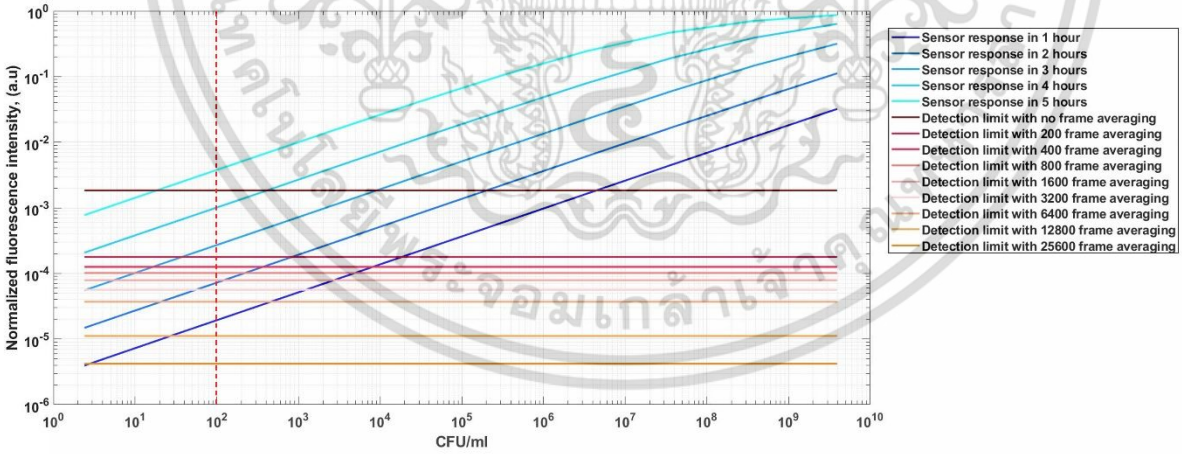

Figure 4.15 Specifies the detection limits for a range of camera frame averages from 0 to 25,600, along with the fluorescence intensity level determined by Equation (8).

The detection limit can be improved by using more average frames; however, doing so comes at the cost of more time spent capturing the video recording to determine the

intensity level. Below 10 seconds of read-out picture data are typically used to read a barcode or a QR code [42]. The underlying detection limit for the suggested method is established in this study using the frame averaging 200 frames per data point, or 6.67 seconds of video recording at a frame rate of 30 frames per second. Due to the increased quantity of produced 4MU, the detection limit of 100 CFU/ml, as reported in the regulation EC No. 2073/2005 for food safety and microbiological safety by the Health Protection Agency (UK), could be achieved at the measuring time of 2 hours and 40 minutes. The World Health Organization (WHO) reported that drinking water safety standards [79] specify that coliform contamination must be below 10 CFU/ml and 1 CFU/ml for medium risk and low risk of fecal contamination, respectively. As depicted in Figure 4.15, the detection limits of 10 CFU/ml and 1 CFU/ml may be reached for experiments spanning 3 hours 25 minutes and 4 hours 10 minutes, respectively.

The enhancement limit for the frame averaging technique, which is 4.2×10^{-6} for the blue fluorescence intensity level when averaging at 25,600 frames, or a 14-minute readout period, is apparent. In other words, capturing videos without a smartphone stand is impractical since it takes so long to hold the camera still. Above 25,600 frames, the amount of averaging frames did not further increase the detection limit. Within an hour of the experiment, this hard video recording can reach the detection limit of < 10 CFU/ml. Therefore, there is a trade-off between the measurement detection limit, readout time, and response time.

4.6 Model evaluation

4.6.1 Unit conversion

In this experiment, the SPR response of *E. coli* detection, optical layers, and refractive indices was extracted from the recent experimental results for measuring various *E. coli* concentrations using a Kretschmann-based wavelength scanning SPR system have been published by Vaisocherová-Lsalová *et al.* [80]. The extracted result is shown in Table 4.1. The experimental setup used in Vaisocherová-Lsalová *et al.* [80] included BK7 glass, a Ti adhesion layer of 5 nm, and uniform gold at a thickness of 50 nm. There were two binding layer cases reported in the article:

1. In Vaisocherová-Lsalová *et al.* [80] article, the layers were formed with a single layer with h_b of 34 nm thickness and n_b of 1.45, made of 12 nm of poly (3-acryloyl amino-propyl) -(2-carboxy-ethyl)-dimethylammonium) or pCBAA, and 10 nm of antibodies.
2. The modeled binding layer was h_b of 90 nm thickness of pCBAA, and n_b was 1.45 in the second case.

Table 4.1 Show data of *E. coli* concentration in CFU/ml unit with the plasmonic wavelength shift $\Delta\lambda_{sp}$ in nm

CFU/ml [80]	$\Delta\lambda_{sp}$ (nm) [80]
1.1×10^4	0.05
4.0×10^4	0.10
1.1×10^5	0.20
8.0×10^5	0.30
1.1×10^6	0.60
8.0×10^6	1.30
1.1×10^7	1.50
1.1×10^8	4.40

To find the relationship between *E. coli* concentration and cell distance between unit cells, the different *E. coli* concentrations, d_s, the relationship of d_s value and its plasmonic wavelength shift $\Delta\lambda_{sp}$ were plotted and depicted in Figure 4.16a. The logarithmic function was employed with linear equation curve fitting to find the relationship equation as expressed in Equation (14) with the coefficient of determination R^2 of 0.99. The $\Delta\lambda_{sp}$ acquired from VaisocherováLsalová *et al.* [80] can be substituted in Equation (15) to obtain d_s and shown in the Table 4.2 at 3rd column corresponding $\Delta\lambda_{sp}$ from the model can be found in the 4th column.

$$\log(d_s) = -1.0013681 \log(\Delta\lambda_{sp}) + 2.0123733 \quad (15)$$

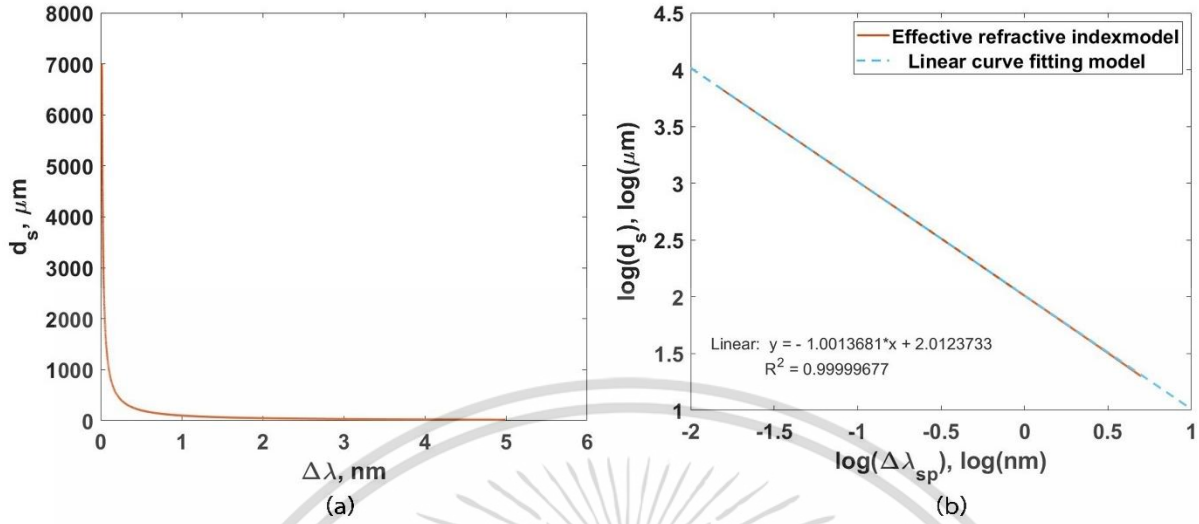

Figure 4.16 Show (a) the relationship between $\Delta\lambda_{sp}$ and its $\boldsymbol{d_s}$ value; (b) relationship of Figure 4.16(a) in logarithmic scale with linear curve fitting function.

Table 4.2 Show the SPR response for various *E. coli* concentrations under the experimental case1

CFU/ml from the article [80]	$\Delta\lambda_{sp}$ (nm) from the article [80]	Equivalent d_s (μm)	$\Delta\lambda_{sp}$ (nm) model
$1.1x10^4$	0.05	2062.0400	0.05
$4.0x10^4$	0.10	1030.0200	0.10
$1.1x10^5$	0.20	514.9600	0.20
$8.0x10^5$	0.30	342.8409	0.30
$1.1x10^6$	0.60	170.8035	0.60
$8.0x10^6$	1.30	78.3732	1.30
$1.1x10^7$	1.50	67.8639	1.50
$1.1x10^8$	4.40	22.7321	4.40

Then the data in Table 4.2 allows us to discover the relationship between CFU/ml (the 1st column) and $\boldsymbol{d_s}$ (the 3rd column) which showed the plotted relationship in Figure 4.17. The data in Table 4.2 were approximated from experimental results, although it is crucial to note that there may be discrepancies in the $\Delta\lambda_{sp}$ data reading. The significant linear

relationship between the CFU/ml and d_s logarithm scale, however, is shown in Figure 4.17 and is stated in Equation (16) with an R^2 of 0.9871.

$$\log(d_s) = -1.0013828 \log(\Delta\lambda_{sp}) + 2.011056578 \quad (16)$$

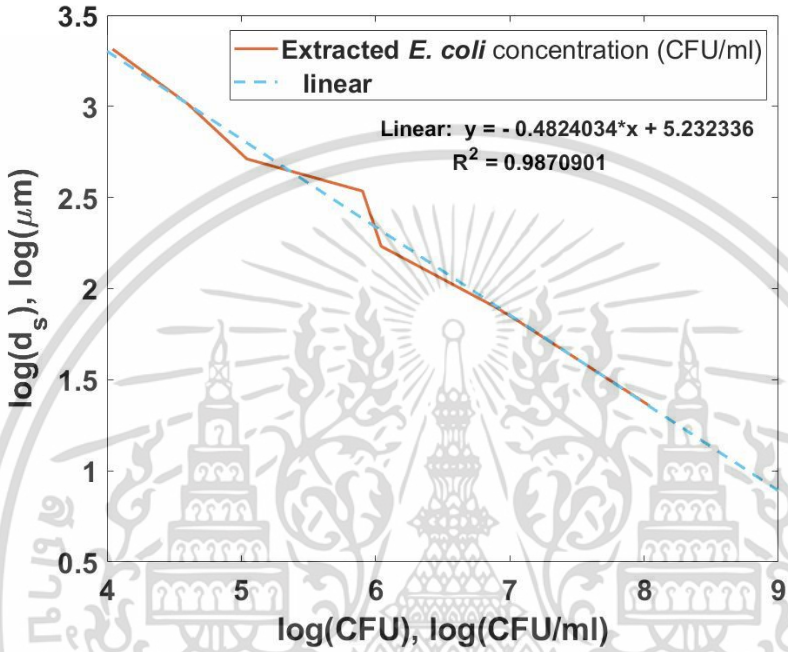

Figure 4.17 Show the relationship between *E. coli* concentration in CFU/ml unit and d_s

According to Equation (16), we were able to discrepancies brought on by the approximate reading graph data from the article, as presented in Table 4.3. The new 3rd column data of Table 4.3 presents the adjusted d_s values determined by Equation (6); therefore, the new corresponding $\Delta\lambda_{sp}$ data can be found in the new 4th column. Equation (5) can be used to determine the cell density levels for each d_s, which are shown in the 5th column of Table 4.3. A corresponding change in the sample region's refractive index is depicted in Figure 4.18 and Table 4.3, 6th column. This change has the same $\Delta\lambda_{sp}$ shifts as the effective refractive index model. Note that the RIU sensitivity should be around 10^{-5} RIU for intensity detection.

Table 4.3 Show the SPR response for various *E. coli* concentrations under the experimental case1 with adjusted $\boldsymbol{d_s}$ and $\Delta\lambda_{sp}$ model values

CFU/ml from the article [80]	$\Delta\lambda_{sp}$ (nm) from the article [80]	New Equivalent d_s (μm)	New $\Delta\lambda_{sp}$ (nm) model	Cell density in cells/μm^2	Equivalent RIU bulk sensitivity
1.1×10^{4}	0.05	1917.5838	0.0539	260.61	2.14×10^{-5}
4.0×10^{4}	0.10	1028.6948	0.1005	485.58	3.96×10^{-5}
1.1×10^{5}	0.20	631.4674	0.1636	790.55	5.78×10^{-5}
8.0×10^{5}	0.30	242.4741	0.4249	2053.61	1.06×10^{-4}
1.1×10^{6}	0.60	207.9446	0.4951	2392.98	1.16×10^{-4}
8.0×10^{6}	1.30	79.8476	1.2794	6184.48	2.02×10^{-4}
1.1×10^{7}	1.50	68.4769	1.4902	7196.64	2.20×10^{-4}
1.1×10^{8}	4.40	22.5497	4.4449	21231.69	3.95×10^{-4}

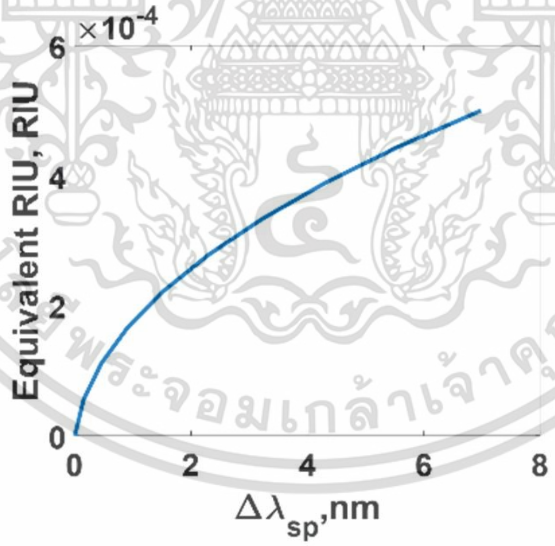

Figure 4.18 Equivalent $\Delta\lambda_{sp}$ in RIU unit

4.6.2 Cross-validation of the model

We have established the relationship between the effective refractive index model parameter $\boldsymbol{d_s}$ and the *E. coli* concentration by a cross-validation or reverse-engineering

procedure, the first case of experimental results published by Vaisocherová-Lsalová *et al.* [80]. Of course, validating the obtained model with an independent measurement is essential in order to determine whether the model can accurately predict the SPR response under various operating conditions and settings. Another set of studies was published by Vaisocherová-Lsalová *et al.* [80], employing 80 nm of pCBAA layer as the experimental case (2) instead of 24 nm. For the 80 nm of pCBAA case, we performed a forward problem to calculate the $\Delta\lambda_{sp}$ from the effective refractive index model; the results are shown in the fourth column of Table 4.4 in comparison to the experimental $\Delta\lambda_{sp}$ obtained from Vaisocherová-Lsalová *et al.* [80] and shown in the second column of Table 4.4. The table shows that the model and experimental results correspond quite well. We also reported the comparable RIU that corresponds to the bulk sensitivity measurement.

Table 4.4 Shows the SPR response for various *E. coli* concentrations under the experimental case2

CFU/ml from the article [80]	$\Delta\lambda_{sp}$ (nm) from the article [80]	Equivalent d_s (μm)	$\Delta\lambda_{sp}$ (nm) model	Cell density in cells/μm^2	Equivalent RIU bulk sensitivity
1.1x10^4	0.04	1917.5838	0.04	260.61	3.28×10^{-5}
4.0x10^4	0.07	1028.6948	0.07	485.58	5.24×10^{-5}
1.1x10^5	0.10	631.4674	0.11	790.55	7.29×10^{-5}
8.0x10^5	0.30	242.4741	0.30	2053.61	1.30×10^{-4}
1.1x10^6	0.40	207.9446	0.35	2392.98	1.43×10^{-4}
8.0x10^6	0.90	79.8476	0.90	6184.48	2.45×10^{-4}
1.1x10^7	1.30	68.4769	1.04	7196.64	2.65×10^{-4}
1.1x10^8	3.10	22.5497	3.10	21231.69	4.74×10^{-4}

4.7 Sensitivity and detection limit

After that, the sensitivity was calculated by plotting a linear sensor response with the $\Delta\lambda_{sp}$ with the *E. coli* concentration CFU/ml from the data from the model in Tables 4.3 and 4.4, as depicted in Figure 4.19. The sensitivity is indicated by the slope of Figure 4.19, which equal to 0.4849 $\frac{nm \cdot ml}{CFU}$ with the coefficient of determination R^2 of 0.9997 for the experiment

1st case that h_b of 24 nm and 0.4768 $\frac{nm \cdot ml}{CFU}$ with the coefficient of determination R^2 of 0.9997 for the experiment 2nd case that h_b of 80 nm. Consequently, the binding site layer's height (h_b) could be affected to decrease the sensitivity, so it is suggested to use a binding layer thickness that is as thin as possible.

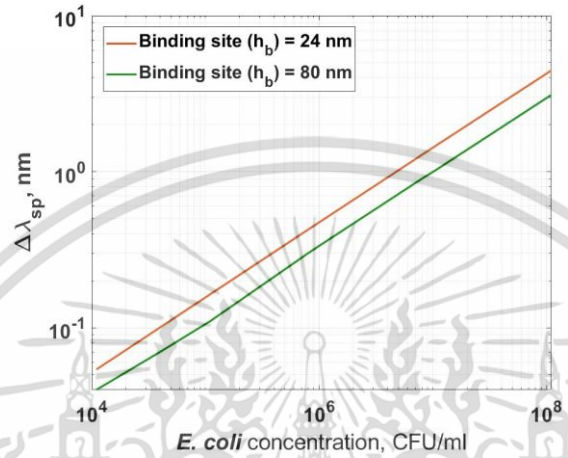

Figure 4.19 Show the sensitivity of SPR wavelength scanning response of h_b=24 nm and h_b=80 nm cases.

Figure 4.20 shows the relationship between the corresponding RIU bulk sensitivity and *E. coli* concentration in CFU/ml can also be used to determine the detection limit. The limit of detection for the h_b of 24 nm and 80 nm experimental cases, respectively, were estimated by extrapolation and polynomial curve fitting to be equal to $10^{3.424}$ CFU/ml and $10^{2.807}$ CFU/ml.

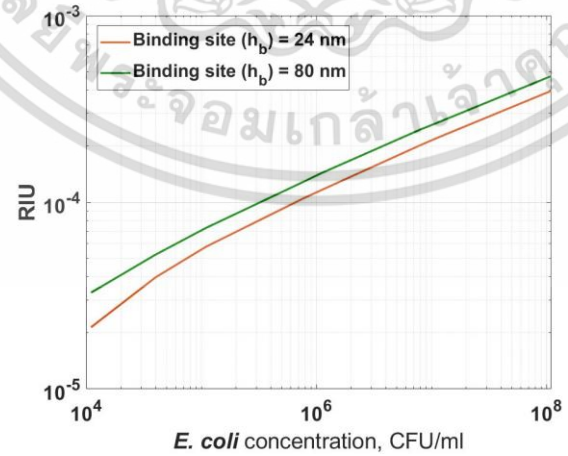

Figure 4.20 Show the correlation between *E. coli* concentration in CFU/ml with RIU response for h_b of 24 nm and 80 nm experimental cases to determine the limit of detection

CHAPTER 5
CONCLUSION

This thesis research has proposed the *E. coli* detection method by measuring the fluorescence product of 4MU from the catalytic reaction that occurs under the MUG-suspended gelatin microfluidic channels, which is cost-effective and environmentally friendly. The blue fluorescence molecule 4MU can be used to quantify *E. coli* due to the enzymatic reaction between the MUG and the GUD secreted by *E. coli*. The MUG-suspended gelatin fluidic channels, the UV light source, and the smartphone were the components of my experimental setup, which was used to record the blue fluorescence light emitted by the 4MU product. The experiment was done by fed distilled water as a negative control, 1700 U/ml of the GUD enzyme as a positive control, and cultured *E. coli* at varying concentrations into the MUG-suspended gelatin fluidic channels and observing the blue fluorescence emitted under the UV light source in the dark room. Compared to the commercial GUD enzyme and the GUD secreted by culturing *E. coli*, which both showed high fluorescence emissions, there was no blue fluorescence emission in the distilled water condition. These results indicated that the enzymatic reaction produced 4MU is available for quantifying *E. coli* in a sample due to the diffusion and the enzymatic reaction mechanism to form the enzyme-substrate complex, the sensing platform required at least 2 hours for fluorescence emission. According to the identical experiments that were also performed using a fluorescence spectrophotometer, the fluidic channels responded similarly to the full-scale cuvette-based measurement. Still, a fluidic channel approach required a longer reaction time. By analyzing the noise and variations in optical intensity, we could determine the standard deviation of the recorded blue fluorescence, which allowed us to discuss the detection limit of the proposed methodology. With a measurement time of 4 hours 10 minutes for the 1 CFU/ml detection limit and 2 hours 40 minutes for the 100 CFU/ml detection limit, and a sensor readout time under 7 seconds, the proposed method can achieve the detection

limit of 1-100 CFU/ml following drinking water standards of the WHO and food safety standards of the Health Protection Agency (UK) and the regulation EC No. 2073/2005.

This thesis also proposed a theoretical framework for analyzing the sensitivity and detection limit of the SPR measurement for detecting *E. coli* quantitatively. This thesis has also proposed a straightforward optical model that utilizes the effective refractive index theory to reduce the complexity of simulating microbes. The experiment results and the model showed good agreement. The detection limit and estimated sensitivity were within the parameters indicated in the thesis. I have discovered through the investigation that the thickness of the binding site may decrease the sensitivity. The detection limit range is between $10^{2.807}$ and $10^{3.424}$ CFU/ml.

REFERENCES

[1] M. Varshney, Y. Li, B. Srinivasan, and S. Tung, "A label-free, microfluidics and interdigitated array microelectrode-based impedance biosensor in combination with nanoparticles immunoseparation for detection of Escherichia coli O157:H7 in food samples," *Sensors and Actuators B: Chemical,* vol. 128, no. 1, pp. 99-107, 2007/12/12/ 2007, doi: https://doi.org/10.1016/j.snb.2007.03.045.

[2] R. L. Buchanan and M. P. Doyle, "Foodborne disease significance of Escherichia coli O157: H7 and other enterohemorrhagic *E. coli*," *Food technology (Chicago),* vol. 51, no. 10, pp. 69-76, 1997.

[3] N. Heredia and S. García, "Animals as sources of food-borne pathogens: A review," *Animal nutrition,* vol. 4, no. 3, pp. 250-255, 2018.

[4] S.-C. Yang, C.-H. Lin, I. A. Aljuffali, and J.-Y. Fang, "Current pathogenic Escherichia coli foodborne outbreak cases and therapy development," *Archives of microbiology,* vol. 199, no. 6, pp. 811-825, 2017.

[5] N. Allocati, M. Masulli, M. F. Alexeyev, and C. Di Ilio, "Escherichia coli in Europe: an overview," *International journal of environmental research and public health,* vol. 10, no. 12, pp. 6235-6254, 2013.

[6] H. Karch *et al.*, "The enemy within us: lessons from the 2011 European Escherichia coli O104: H4 outbreak," *EMBO molecular medicine,* vol. 4, no. 9, pp. 841-848, 2012.

[7] U. ISO, "Water Quality. Enumeration of Escherichia Coli and Coliform Bacteria. Part 1: Membrane Filtration Method for Waters with Low Bacterial Background Flora," ed: International Organization for Standardization Geneva, Switzerland, 2014.

[8] S. T. Odonkor and T. Mahami, "Escherichia coli as a tool for disease risk assessment of drinking water sources," *International Journal of Microbiology,* vol. 2020, 2020.

[9] A. Deisingh and M. Thompson, "Strategies for the detection of Escherichia coli O157: H7 in foods," *Journal of applied microbiology,* vol. 96, no. 3, pp. 419-429, 2004.

[10] H. Zhu, U. Sikora, and A. Ozcan, "Quantum dot enabled detection of Escherichia coli using a cell-phone," *Analyst,* vol. 137, no. 11, pp. 2541-2544, 2012.

[11] S. Mura *et al.*, "FTIR nanobiosensors for Escherichia coli detection," *Beilstein journal of nanotechnology,* vol. 3, no. 1, pp. 485-492, 2012.

[12] Y.-W. Zhao, H.-X. Wang, G.-C. Jia, and Z. Li, "Application of aptamer-based biosensor for rapid detection of pathogenic Escherichia coli," *Sensors,* vol. 18, no. 8, p. 2518, 2018.

[13] D. Wildeboer, L. Amirat, R. G. Price, and R. A. Abuknesha, "Rapid detection of Escherichia coli in water using a hand-held fluorescence detector," *Water research,* vol. 44, no. 8, pp. 2621-2628, 2010.

[14] S. B. March and S. Ratnam, "Sorbitol-MacConkey medium for detection of Escherichia coli O157: H7 associated with hemorrhagic colitis," *Journal of clinical microbiology,* vol. 23, no. 5, pp. 869-872, 1986.

[15] M. S. Cheng, S. H. Lau, V. T. Chow, and C.-S. Toh, "Membrane-based electrochemical nanobiosensor for Escherichia coli detection and analysis of cells viability," *Environmental science & technology,* vol. 45, no. 15, pp. 6453-6459, 2011.

[16] L. Guo *et al.*, "Turn-on fluorescence detection of β-glucuronidase using RhB@ MOF-5 as an ultrasensitive nanoprobe," *Sensors and Actuators B: Chemical,* vol. 295, pp. 1-6, 2019.

[17] J. W. Tapsall and C. J. McIver, "β-d-Glucuronidase activity among prototrophic and auxotrophic variants of Escherichia coli and other Enterobacteriaceae commonly implicated in urinary tract infections," *Diagnostic microbiology and infectious disease,* vol. 22, no. 3, pp. 261-266, 1995.

[18] K. A. Biernat *et al.*, "Structure, function, and inhibition of drug reactivating human gut microbial β-glucuronidases," *Scientific reports,* vol. 9, no. 1, pp. 1-15, 2019.

[19] R. Flores, J. Shi, M. H. Gail, P. Gajer, J. Ravel, and J. J. Goedert, "Association of fecal microbial diversity and taxonomy with selected enzymatic functions," *PloS one,* vol. 7, no. 6, p. e39745, 2012.

[20] P. Feng, R. Lum, and G. W. Chang, "Identification of uidA gene sequences in beta-D-glucuronidase-negative Escherichia coli," *Applied and environmental microbiology,* vol. 57, no. 1, pp. 320-323, 1991.

[21] L. Pala, T. Sirec, and U. Spitz, "Modified enzyme substrates for the detection of bacteria: a review," *Molecules,* vol. 25, no. 16, p. 3690, 2020.

[22] N. Hesari, A. Alum, M. Elzein, and M. Abbaszadegan, "A biosensor platform for rapid detection of *E. coli* in drinking water," *Enzyme and microbial technology,* vol. 83, pp. 22-28, 2016.

[23] M. G. Somekh and S. Pechprasarn, "Surface plasmon, surface wave, and enhanced evanescent wave microscopy," in *Handbook of Photonics for Biomedical Engineering*: Springer Netherlands, 2017, pp. 503-543.

[24] S. Wang *et al.*, "The development of a portable SPR bioanalyzer for sensitive detection of escherichia coli O157: H7," *Sensors,* vol. 16, no. 11, p. 1856, 2016.

[25] Y. Wang, Z. Ye, C. Si, and Y. Ying, "Subtractive inhibition assay for the detection of *E. coli* O157: H7 using surface plasmon resonance," *Sensors,* vol. 11, no. 3, pp. 2728-2739, 2011.

[26] M. Safavieh, S. Nahar, M. Zourob, and M. Ahmed, "Microfluidic biosensors for high throughput screening of pathogens in food," in *High Throughput Screening for Food Safety Assessment*: Elsevier, 2015, pp. 327-357.

[27] T. Bintsis, "Foodborne pathogens," *AIMS microbiology,* vol. 3, no. 3, p. 529, 2017.

[28] J. P. Nataro and J. B. Kaper, "Diarrheagenic escherichia coli," *Clinical microbiology reviews,* vol. 11, no. 1, pp. 142-201, 1998.

[29] A. Kulkarni. "What does an *E. coli* bacteria look like under a microscope?" https://www.quora.com/What-does-an-E-Coli-bacteria-look-like-under-a-microscope

[30] M. Nurliyana *et al.*, "The detection method of Escherichia coli in water resources: A review," in *Journal of Physics: Conference Series*, 2018, vol. 995, no. 1: IOP Publishing, p. 012065.

[31] L. Y. Yeo, H. C. Chang, P. P. Chan, and J. R. Friend, "Microfluidic devices for bioapplications," *small,* vol. 7, no. 1, pp. 12-48, 2011.

[32] F. Bragheri, R. M. Vázquez, and R. Osellame, "Microfluidics," in *Three-dimensional microfabrication using two-photon polymerization*: Elsevier, 2020, pp. 493-526.

[33] S. Haeberle and R. Zengerle, "Microfluidic platforms for lab-on-a-chip applications," *Lab on a Chip,* vol. 7, no. 9, pp. 1094-1110, 2007.

[34] H. Andersson and A. Van den Berg, "Microfluidic devices for cellomics: a review," *Sensors and actuators B: Chemical,* vol. 92, no. 3, pp. 315-325, 2003.

[35] A.-G. Niculescu, C. Chircov, A. C. Bîrcă, and A. M. Grumezescu, "Fabrication and applications of microfluidic devices: A review," *International Journal of Molecular Sciences,* vol. 22, no. 4, p. 2011, 2021.

[36] M. Aljabri *et al.*, "Canine impaction classification from panoramic dental radiographic images using deep learning models," *Informatics in Medicine Unlocked,* vol. 30, p. 100918, 2022.

[37] J. Alipal *et al.*, "A review of gelatin: Properties, sources, process, applications, and commercialisation," *Materials Today: Proceedings,* vol. 42, pp. 240-250, 2021.

[38] Bakerydeco. "Gelatin powder." https://www.bakerydeco.com/products/gelatin-powder/

[39] Wikipedia. "Ultraviolet." https://en.wikipedia.org/wiki/Ultraviolet (accessed.

[40] N. A. a. Space. "Ultraviolet Waves." https://science.nasa.gov/ems/10_ultravioletwaves (accessed.

[41] J. Lucas, "What Is Ultraviolet Light?," 2017, September 16. [Online]. Available: https://www.livescience.com/50326-what-is-ultraviolet-light.html.

[42] Wikipedia. "Logistic funcation." https://en.wikipedia.org/wiki/Logistic_function

[43] D. Kucharavy and R. De Guio, "Application of logistic growth curve," *Procedia engineering,* vol. 131, pp. 280-290, 2015.

[44] M. Manafi, "Detection of specific taxa using chromogenic and fluorogenic media," *Manual of Environmental Microbiology,* pp. 2.1. 1-1-2.1. 1-9, 2016.

[45] GIBCO, *Cell culture basics*.

[46] S. Aryal. "Spread Plate Technique- Principle, Procedure and Uses." https://microbiologyinfo.com/spread-plate-technique-principle-procedure-and-uses/#:~:text=The%20spread%20plate%20technique%20involves,absorb (accessed.

[47] N. Rijal. "Spread Plate Technique: Principle, Procedure, Results." https://microbeonline.com/spread-plate-technique/

[48] A. Ryer, U. Light, and V. Light, "Light measurement handbook," 1997.

[49] R. M. Bakker *et al.*, "Magnetic and electric hotspots with silicon nanodimers," *Nano Letters,* vol. 15, no. 3, pp. 2137-2142, 2015.

[50] K. Academy. "Electric and magnetic fields." https://www.khanacademy.org/science/hs-physics/x215e29cb31244fa1:types-of-interactions/x215e29cb31244fa1:electric-and-magnetic-fields/a/electric-and-magnetic-fields#:~:text=A%20magnetic%20field%20is%20a,on%20an%20object%20in%20space.&text=A%20electric%20field%20is%20a,any%20given%20point%20in%20space.&text=Current%20is%20the%20rate%20of%20charge%20moving%20past%20a%20region.

[51] G. Verhoeven and V. Archaeology, "The reflection of two fields–Electromagnetic radiation and its role in (aerial) imaging," *AARGnews,* vol. 55, no. 55, pp. 10-18, 2017.

[52] E. Britannica. "refractive index." https://www.britannica.com/science/refraction

[53] Byjus. "Reflection Of Light." https://byjus.com/physics/reflection-of-light/#:~:text=When%20a%20ray%20of%20light,is%20called%20the%20reflected%20ray.

[54] S. L. Hub. "Refraction of light." https://www.sciencelearn.org.nz/resources/49-refraction-of-light

[55] M. W. Davidson. "Refractive Index (Index of Refraction)." https://www.microscopyu.com/microscopy-basics/refractive-index-index-of-refraction

[56] OptoSigma. "OPTICS & OPTICAL COATINGS." https://www.optosigma.com/us_en/support/tutorial/optics-and-optical-coatings/technical-referance/optical-coatings

[57] E. Optic. "Introduction to Polarization." https://www.edmundoptics.com/knowledge-center/application-notes/optics/introduction-to-polarization/

[58] S. Abbas, S. Salman, and A. Abbas, "Studying of the polarization modes TE and TM for oblique incidence of light on thin films," *Digest Journal of Nanomaterials and Biostructures,* vol. 16, no. 2, pp. 647-657, 2021.

[59] J. Homola, S. S. Yee, and G. Gauglitz, "Surface plasmon resonance sensors," *Sensors and actuators B: Chemical,* vol. 54, no. 1-2, pp. 3-15, 1999.

[60] Y. Chen and H. Ming, "Review of surface plasmon resonance and localized surface plasmon resonance sensor," *Photonic Sensors,* vol. 2, no. 1, pp. 37-49, 2012.

[61] B. Liedberg, C. Nylander, and I. Lunström, "Surface plasmon resonance for gas detection and biosensing," *Sensors and actuators,* vol. 4, pp. 299-304, 1983.

[62] A. M. Craciun, M. Focsan, K. Magyari, A. Vulpoi, and Z. Pap, "Surface plasmon resonance or biocompatibility—key properties for determining the applicability of noble metal nanoparticles," *Materials,* vol. 10, no. 7, p. 836, 2017.

[63] K. Nagata and H. Handa, "Real-time analysis of biomolecular interactions," *Applications of Biacore,* pp. 13-22, 2000.

[64] C. Lochotinunt, T. Teechot, S. Pechprasarn, and T. Treebupachatsakul, "Microfluidic Channel from Gelatin Using Laser Printer," in *2020 International Conference on e-Health and Bioengineering (EHB)*, 2020: IEEE, pp. 1-4, doi: 10.1109/EHB50910.2020.9280262.

[65] P. B. Johnson and R.-W. Christy, "Optical constants of the noble metals," *Physical review B,* vol. 6, no. 12, p. 4370, 1972.

[66] D. Z. Stupar *et al.*, "Remote monitoring of water salinity by using side-polished fiber-optic U-shaped sensor," in *2012 15th International Power Electronics and Motion Control Conference (EPE/PEMC)*, 2012: IEEE, pp. LS4c. 4-1-LS4c. 4-5.

[67] A. E. Balaev, K. Dvoretski, and V. A. Doubrovski, "Refractive index of Escherichia coli cells," in *Saratov Fall Meeting 2001: Optical Technologies in Biophysics and Medicine III*, 2002, vol. 4707: SPIE, pp. 253-260.

[68] M. Riley, "Correlates of smallest sizes for microorganisms," in *Size limits of very small microorganisms: proceedings of a workshop*, 1999, vol. 3: National Academies Press Washington DC, USA, p. 21.

[69] S. Sasivimolkul, S. Pechprasarn, and M. G. Somekh, "Analysis of open grating-based Fabry–Pérot resonance structures with potential applications for ultrasensitive refractive index sensing," *IEEE Sensors Journal,* vol. 21, no. 9, pp. 10628-10636, 2021.

[70] C. Liu *et al.*, "Design and theoretical analysis of a photonic crystal fiber based on surface plasmon resonance sensing," *Journal of Nanophotonics,* vol. 9, no. 1, p. 093050, 2015.

[71] H. Fujikawa, A. Kai, and S. Morozumi, "A new logistic model for Escherichia coli growth at constant and dynamic temperatures," *Food microbiology,* vol. 21, no. 5, pp. 501-509, 2004.

[72] E. Atolia *et al.*, "Environmental and physiological factors affecting high-throughput measurements of bacterial growth," *Mbio,* vol. 11, no. 5, pp. e01378-20, 2020.

[73] O. Burggraaff *et al.*, "Standardized spectral and radiometric calibration of consumer cameras," *Optics express,* vol. 27, no. 14, pp. 19075-19101, 2019.

[74] R. F. Chen, "Fluorescent pH indicator. Spectral changes of 4-methylumbelliferone," *Analytical Letters,* vol. 1, no. 7, pp. 423-428, 1968.

[75] K. Matsumura, P. Rolfe, J. Lee, and T. Yamakoshi, "iPhone 4s photoplethysmography: which light color yields the most accurate heart rate and normalized pulse volume using the iPhysioMeter application in the presence of motion artifact?," *PloS one,* vol. 9, no. 3, p. e91205, 2014.

[76] P. Hu, P. H. Pathak, X. Feng, H. Fu, and P. Mohapatra, "Colorbars: Increasing data rate of led-to-camera communication using color shift keying," in *proceedings of the 11th ACM conference on Emerging Networking experiments and technologies*, 2015, pp. 1-13.

[77] K. Thadson, S. Sasivimolkul, P. Suvarnaphaet, S. Visitsattapongse, and S. Pechprasarn, "Measurement precision enhancement of surface plasmon resonance based angular scanning detection using deep learning," *Scientific Reports,* vol. 12, no. 1, pp. 1-14, 2022.

[78] K. Thadson, S. Visitsattapongse, and S. Pechprasarn, "Deep learning-based single-shot phase retrieval algorithm for surface plasmon resonance microscope based refractive index sensing application," *Scientific Reports,* vol. 11, no. 1, pp. 1-14, 2021.

[79] P. Gwimbi, "The microbial quality of drinking water in Manonyane community: Maseru District (Lesotho)," *African health sciences,* vol. 11, no. 3, 2011.

[80] H. Vaisocherová-Lísalová *et al.*, "Low-fouling surface plasmon resonance biosensor for multi-step detection of foodborne bacterial pathogens in complex food samples," *Biosensors and Bioelectronics,* vol. 80, pp. 84-90, 2016.

BIOGRAPHY

Name	Mr. Chanin Lochotinunt
Date of Birth	5 January 1999
Address	33 Soi 5, Patan Road, Patan Sub-district,
	Muang District, Chiang Mai, 50300
Education	2020 Bachelor of Engineering Biomedical Engineering (First Class Honor)
	King Mongkut's Institute of Technology Ladkrabang
Specialized field	1.) Biosensor
	2.) Microbial detection
	3.) Microfluidic channel
Publications and Awards	
2018-2022	- The second award of the Medical devices ASEAN contest 2018
	- Honorable mention award of Medical devices ASEAN contest 2019
	- Gold medal award in World Invention Creativity Olympic (WICO) 2019
	- Publication "Neurofeedback system" in BMEiCON 2019
	- Publication "Microfluidic channel from Gelatin by Laser printer" in EHB 2020
Present	- Publication "Gelatin-based microfluidic channel for quantitative *E. coli* detection using blue fluorescence of 4-methyl-umbelliferone product and a smartphone camera" in IEEE Sensor Journal
	- Publication " Detection Limit of Surface Plasmon Resonance Sensor for Quantitative Foodborne *E. coli* Detection Using Effective Refractive Index Theory" in BMEiCON 2021
	- Publication " Classification model for predicting inflammation of the urinary bladder and acute nephritis of the renal pelvis" in BMEiCON 2022